THE PENNSYLVANIA STATE UNIVERSITY
SCHREYER HONORS COLLEGE

DEPARTMENT OF BIOENGINEERING

A STUDY IN THE DESIGN OF AN ACCELERATED WEAR TESTER THAT IS COMPATIBLE WITH A
PARTICLE IMAGE VELOCIMETRY AND HIGH SPEED CAMERA SETUP

EDWARD A. BROWN
SUMMER 2015

A thesis
submitted in partial fulfillment
of the requirements
for a baccalaureate degree
in Bioengineering
with honors in Science

Reviewed and approved* by the following:

Keefe B. Manning
Associate Professor of Biomedical Engineering
Thesis Supervisor/Honors Adviser

William Hancock
Professor of Biomedical Engineering
Faculty Reader

* Signatures are on file in the Schreyer Honors College.

Abstract

Cardiovascular disease (CVD) is the leading cause of death in the United States. A subset of CVD affects the valves of the heart (HVD). Due to the aging population's susceptibility to HVD, it is a growing concern. Heart valve replacement is often necessary if the valve is beyond repair. There are two main categories of artificial heart valves that can be used for a replacement, mechanical and bioprosthetic. Although there have been many advances in artificial heart valve technology, there are still many problems that need to be addressed. One major problem for bioprosthetic heart valves is deterioration . This study aims to design an accelerated wear tester (AWT) that is compatible with a particle image velocimetry and high speed camera set up so that bioprosthetic heart valve deterioration can be studied at an accelerated rate. By using SolidWorks, a single chamber AWT was designed and its materials were modeled to determine if it could withstand the stresses of testing a heart valve at an accelerated rate. The design of the AWT needed to be able to meet FDA requirements for *in vitro* bioprosthetic heart valve testing. Simulations were run to determine if the AWT could test a bioprosthetic heart valve over 200 million open and close cycles, having the valve fully open and close during each cycle, while maintaining a minimum average transvalvular pressure of 100 mmHg during valve closure. Based on the initial tests, the AWT's acrylic walls underwent loading stresses of 0.99 MPa, which is much smaller than acrylic's fatigue life of 38 MPa. This means that the flow chamber walls will not break or crack while testing the heart valve over the valve's entire life span. The pressures induced by the AWT's piston motor during its down-stroke (~135 mmHg) and its up-stroke (~ -120 mmHg) were large enough to fully open and close the valve during each heart beat. The piston's up-stroke created a transvalvular pressure drop

of 120 mmHg during valve closure, proving that the AWT will be able to meet all the FDA requirements for testing bioprosthetic heart valves. Future studies will need to be carried out to physically building the AWT.

TABLE OF CONTENTS

List of Figures

List of Tables

List of Symbols

EOA	Effective orifice area
Q_{rms}	Root mean square of the systolic/diastolic flow rate
$\Delta\bar{p}$	Mean systolic/diastolic pressure drop
DVI	Doppler velocity index
V_{LVOT}	Velocity in the left ventricular outflow tract
V_{PV}	Velocity through the valve
U	Velocity field
T	Time
P	Pressure
I	Unit diagonal matrix
H	Dynamic viscosity
∇	Del operator
P	Density
$\mathbf{u}_m$	Coordinate system velocity
F_T	Force on valve
N	Unit normal vector
F	Volume force affecting the fluid

Acknowledgements

There have been so many people throughout this project that I would like to express my gratitude towards. First, I would like to thank Dr. Keefe Manning for his insight and wisdom. His encouragement and guidance throughout this whole process pushed me to constantly improve and perfect my work. I would also like to thank Dr. William Hancock and Dr. Yong Wang for their knowledge and their ideas on developing my research, which led to a much more well rounded thesis. Thanks to Dr. Butler for helping with the COMSOL simulations. I would also like to thank the members of the Artificial Heart Lab. Especially Josh Taylor and Kenneth Aycock for introducing me to the basic principles of accelerated wear testing. I would also like to thank the Bioengineering staff especially Gary Meyers, Gene Gerber, and Carol Boring who were always there to help when I ran into any kind of technical difficulties.

I would also like to thank my friends and family for their unconditional love and support during this whole process. Not only did they encourage me and listen to my constant complaints, but also always found a way to pick up my spirits and help me relax exactly when I needed it. This was especially true for my girlfriend Kathleen Ritchie and my parents Christopher and Michele Brown. Thank you all so very much.

Chapter 1

Introduction

1.1 Clinical Need

Cardiovascular disease (CVD) is currently the leading cause of death in the United States and has been the leading cause of death for over 100 years (1). Heart valve disease (HVD) is a subset of CVD that concerns the valves of the heart. HVD can affect any of the four heart valves and is characterized by regurgitation, stenosis, or atresia (2). The most common cause of HVD is the mineralization of the aortic valve, also known as calcific aortic valve disease (3, 4). HVD is commonly treated with medication and lifestyle changes; however, invasive surgery is sometimes required depending on the severity of the patient's HVD. These surgeries can range from valve reconstruction surgery to total valve replacement. The most common cause of such surgeries is aortic stenosis (5, 6, 7). Even with these treatments, HVD affects approximately 2.5% of American adults and has a significant mortality and morbidity rate (8, 9, 10). Risk factors for HVD include high blood pressure, high cholesterol, obesity, smoking, diabetes, and having a family history of cardiovascular disease (2, 11). Age is also a major risk factor for HVD (2, 4). Nkomo reported in 2006 that varying degrees of HVD already affect 13% of people 75 years and older (4). The census bureau also estimates that about one third of the United States population will be 55 years or older by the year 2020 (12). With such a large populace at risk for HVD, there is a huge need for improved HVD treatment. Each year in the United States, 60,000 heart valve replacement surgeries are performed (13). When valve replacement surgery is needed, they tend to have poor results with most patients having a short to midterm

mortality rates (8). These poor outcomes can be due to poor valve biocompatibility, mechanical failure, or thromboembolic complications (14, 15, 16).

1.2 Artificial Heart Valves

Valve replacement surgery has been used as early as the 1960's (13). Artificial heart valves fall into two main categories, mechanical valves and bioprosthetic valves. Within each category there are many different types. Ball and cage valves, tilting disk valves, and bileaflet valves fall into the mechanical heart valve category, while allografts, xenografts, and pericardial xenografts fall into the bioprosthetic valve category, all of which can be seen in Figure 1.2.1 (16, 17).
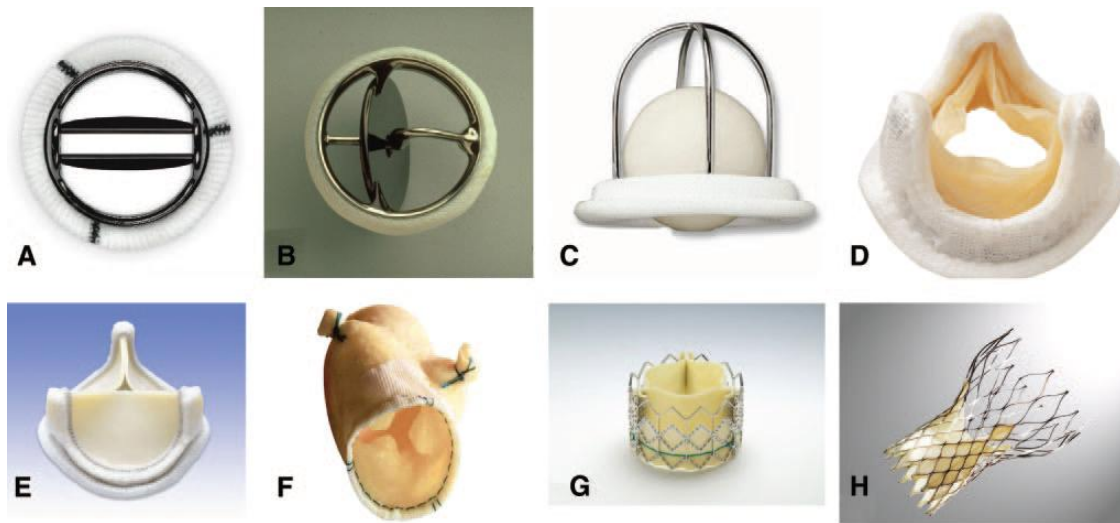
Figure 1.2.1 Different types of artificial heart valves. A, Bileaflet mechanical valve; B, tilting disk mechanical valve; C, caged ball valve; D, stented porcine bioprosthesis; E, stented pericardial bioprosthesis; F, stentless porcine bioprosthesis; G, percutaneous bioprosthesis expanded over a bolloon; H, self-expandable percutaneous bioprosthesis (Figure taken from Ref. 13)

Current day ball and cage valves consist of a silastic ball and a cage formed from metal arches (17). the Starr-Edwards, Magovern-Cromie, DeBakey-Surgitool, and Smeloff-Cutter valves were all developed having this basic design, with only minor variations (18). The first

successful human heart valve replacement surgery used the Starr-Edwards ball and cage valve. This specific valve consisted of a Lucite cage with thick struts and a compression molded silicone-rubber ball (19). Although successful, the valve still had many problems and was changed many times over the next 5 years. The developers of the Starr-Edwards valve realized that the valve must be durable and corrosion resistant so they changed the cage material from Lucite to stainless steel. They also changed the sewing ring from a doughnut shape to a flange shape, making the valve easier to attach and increasing the security of the attachment (19). The turbulent flow caused by the valve was reduced by increasing the valve's orifice-to-ball ratio (20). Finally, after much development, the Starr-Edwards ball and cage valve 6120 series was created and was subsequently used in HVD patients for more than 20 years (21). Tarzia was able to undertake a 31 year valve follow-up on a Starr-Edwards replacement valve patient in 2007. They reported that the explanted valve was free of structural degradation, attesting to the durability of ball and cage valves (23). Although durable, the Starr-Edwards ball and cage valve was prone to thrombus formation, due to their lateral flow field, high transvalvular pressure gradients, and non-physiological surfaces. This often led to device failure and patient death (23).

The tilting disk valve consists of a single disk opening at an angle between 60° and 80°. The disk is secured to central metal supports to keep it from breaking off of the valve housing. The most prevalent type of tilting disk valve is the Medtronic-Hall valve, consisting of an opening angle of 70°-75°, support struts made from titanium, and a polytetrafluoroethylene sewing ring (23, 24, 25). The Medtronic-Hall valve was an improvement to the Starr-Edwards valve, having improved hemodynamics, while retaining the durability that was seen in the Starr-

Edwards valve (24). Other types of tilting disk valves include the Bjork-Shiley and the

Monostrut valves (26). A 25 year patient follow-up was conducted in 2007 by Svennevig *et al.*

finding that of the 816 patients implanted with a Medtronic-Hall valve, there were only 4

occurrences of thrombus formation, a vast improvement to the thrombus prone ball and cage

valves (27).

The bileaflet valve consists of two semilunar disks attached by metal struts, opening at

angles between 75° and 90°. Valves of this type include the ATS Open Pivot, CarboMedics, On-

X, and, the most common, the St. Jude bileaflet valve (23, 26). The St. Jude valve opens at an

angle of 85°, has pivot guards, struts, and orifice projections. These features help to reduce

turbulent flows through the valve (28). Emery *et al*. analyzed patient data between October

1977 and October 2002 to determine long-term feasibility of the St. Jude valve. Of the 4,480

patients in the study, the incidence of thromboembolic events was 1.9%/patient year for aortic

valve replacement patients and 2.8%/patient year for mitral valve replacement patients. One

patient had structural failure occur (29). This data is comparable to that found for the

Medtronic-Hall valve.

Allografts are taken from human cadavers or brain dead organ donors and sterilized

using antibiotic solutions prior to implantation (16). These valves are not commercially

available or mass produced because they are taken from other humans.

Porcine and bovine tissue are used for xenograft bioprostheses and consists of 3 aortic

valve leaflets. Valves of this type include the Freestyle, Epic, Medtronic Hancock II, Mosaic, and

the St. Jude Medical Biocor porcine prosthesis (26). The last of which is widely used when

choosing a bioprosthetic valve for implantation. Patient data between 1983 and 2003 was

analyzed to determine long-term feasibility of the Biocor valve. Of the 1,712 patients in the study, the incidence of thromboembolic events was 1.6%/patient year for aortic valve replacement patients and 2.2%/patient year for mitral valve replacement patients (30). This is better than any of the mechanical valves discussed earlier and is accomplished without the use of lifelong anticoagulation therapy. Valve structural failure, however, occurred in 4 patients, which is a larger occurrence than is seen in all of the mechanical valve studies combined (30). This is due to valve calcification and deterioration which is characteristic of bioprosthetic heart valves.

Porcine and bovine tissue are also used for pericardial xenografts. Using pericardial tissue for valve leaflets improves the hemodynamic performance of the valve compared to normal valve xenografts (31). The ATS 3f, Carpentier-Edwards Perimount, Mitroflow, and Trifecta are all common types of pericardial xenografts (26). Long term outcomes from the Carpentier-Edwards valve found 13 valve structural failures after 17 years (31). This is an improvement compared to first generation pericardial valves; however, is still large compared to the Biocor porcine valve. The Carpentier-Edwards valve exceeds the Biocor porcine valve when it comes to thromboembolic events, having an occurrence of only a 0.003%/patient year (31).

1.3 Bioprosthetic Implantation

Not only are there different types of bioprosthetic valves, there are also different implantation methods that can be used. The most common implantation method is to use a stent attached to a sewing ring. More recently however, valves have been implanted without the use of stents and sewing rings. Surgeons implant the valves by sewing the valve in free

hand. Finally, in a generally new procedure, valves have been implanted percutaneously using a catheter that travels through the femoral artery (17). Each implantation method has its benefits and detriments. Implanting the valve without a stent increases the valve's effective orifice area, improving valve function, however, the procedure is harder to perform compared to using a stent, leading to surgical errors. Implanting the valve percutaneously decreases the risks of aortic valve replacement surgery, but is the most difficult procedure to perform (16, 17).

Each valve type has its own advantages and disadvantages as well. Mechanical valves are very durable and long lasting, however, they have a higher thrombogenicity and patients must take anticoagulation medication for the remainder of their lives. Bioprosthetic valves are more prone to failure due to structural deterioration, however, they have a higher biocompatibility and require little to no medication after the operation (32). These advantages and disadvantages along with a patient's general health prior to valve replacement surgery determine which type valve is implanted.

1.4 Bioprosthetic Valve Function

Two ways bioprosthetic heart valve performance is measured is by using the valve's effective orifice area (EOA) and the valve's regurgitation volume. The effective orifice area measures how effectively the valve opens when blood is being pushed through the valve due to heart contraction. Regurgitant volume is the amount of blood that flows backwards through the valve when it is closed (33). The effective orifice area is calculated using Equation: 1.4.1:

$$EOA \ (cm^2) = \frac{Q_{rms}}{56.1 * \sqrt{\overline{\Delta P}}} \qquad (1.4.1) \qquad (33)$$

Where Q_{rms} is the root mean square of the systolic/diastolic flow rate (cm^3/s) and $\Delta\bar{p}$ is equal to the mean systolic/diastolic pressure drop (mmHg) (33). A low EOA causes a higher workload for the heart, decreasing valve efficiency. A high regurgitant volume decreases the total amount of blood that flows through the valve in one cardiac cycle increasing the hearts workload and decreasing valve efficiency. Therefore, a valve functioning at peak efficiency will have a large EOA and a small regurgitant volume.

Another way to determine valvular function is through the Doppler Velocity Index (DVI). This is a ratio between the proximal velocity in the left ventricular outflow tract compared to the velocity through the valve and can be determined using equation 1.4.2:

$$DVI = \frac{V_{LVOT}}{V_{PV}} \qquad (1.4.2) \qquad (33)$$

Where V_{LVOT} is the velocity in the left ventricular outflow tract and V_{PV} is the velocity through the valve (33). Ideally, a valve should have a DVI of 1. If this quantity is lower, however, it could mean that the valve is no longer functioning properly. This could be due to some sort of obstruction (possibly a thrombus).

1.5 Artificial Heart Valve Complications

As with any new medical technology, artificial heart valves are not without their problems, one of which is biocompatibility. Biocompatibility is a vital aspect of any medical device that contacts the human body affecting device performance, reliability, and safety. Although medical devices are designed to help treat certain diseases, the body often considers the device a foreign material and the patient's immune system will attack it causing the device

to degrade and malfunction over time. Ideally, devices will perform its specific function while simultaneously inducing no negative biological responses from the patient's immune system.

Due to the safety issues seen in artificial heart valves and the drastic consequences that these issues cause, biocompatibility is one of the top priorities when they are designed. If overlooked, the biocompatibility of artificial heart valves can cause thrombus formation which could lead to device failure and patient death. After implantation, patients with prosthetic heart valves are prone to thromboembolic events with an occurrence of 2.3%/patient year (13, 34, 35). Thrombus formation can be caused by the artificial heart valve's abnormal flow fields. These flow fields are normally seen in the valve's hinge region during regurgitant flow.

A small amount of regurgitant flow is often seen as beneficial for its ability to wash away thrombi forming on the valve (33). Most valves are designed to have a small regurgitant volume because of this. Although regurgitant flow is seen as beneficial, non-physiological flow fields often occur during it. In studies characterizing the velocity measurements and flow patterns within the hinge region of mechanical heart valves, it was found that the hinge geometry played a major role in abnormal flow field generation (36, 37, 38, 39). The highest shear stresses occurred during diastole, during which regurgitant flow occurs (39). The turbulent shear stresses found near the hinge region of the valve led to unsteady flow, vortex formation, and zones of stagnation (36, 38, 40). High turbulent shear stresses can cause hemolysis and platelet activation and when combined with the vortex formation and the zones of stagnation, have high probabilities of inducing thrombus formation.

Once activated, platelets accelerate thrombosis (41, 42). Thrombi can impede valve function by occluding the valve orifice. If they embolize, they can also cause the patient to have

a heart attack or a stroke. An electron micrograph image compares conformational changes in inactive and active platelets as seen in Figure 1.5.1.
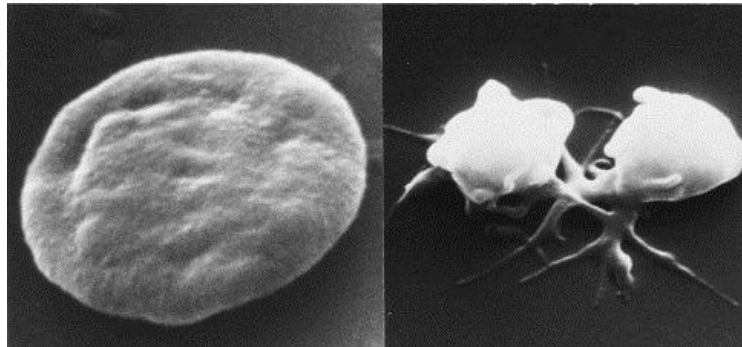
Figure 1.5.1 Electron micrograph of a resting platelet (left) and two activated platelets exhibiting pseudopodia formation (right) (Figure taken from Ref. 43).

Another complication associated with artificial heart valves is unwanted patient hemorrhaging. This is normally due to anticoagulation medications that patients receive in an effort to minimize the chance of thromboembolic events. These events are only seen with mechanical heart valves because patients who have bioprosthetic valves do not need to undergo any kind of anticoagulant therapy (44).

Valve deterioration is another major concern for artificial heart valves. Mechanical heart valves rarely deteriorate due to their high material durability, however, the rate of bioprosthetic heart valve deterioration increases over time. This rate rises dramatically 7 to 8 years after valve implantation. Risk factors leading to valve deterioration include younger patient age, mitral valve positioning, renal insufficiency, and hyperparathyroidism (13). The most common cause of valve failure in bioprosthetic heart valves is calcification (45).

Calcification can be seen histologically on bioprosthetic valves within 3 years; however, calcification has been reported as early as 19 days after implantation (46, 47). Calcification can

cause paravalvular leakage, cusp tears, incompetence, stenosis, and valve stiffening (46, 48, 49). All of these problems lead to impaired valve performance, thrombogenesis, and valve deterioration. Bioprosthetic valves are normally treated with glutaraldehyde to preserve the tissue and decrease valve immunogenicity, however, this treatment also devitalizes the valve's connective tissue (46, 49). Calcification is normally initiated in these devitalized cells because they are unable to pump out calcium from the cytoplasm and inter-cellular structures. This leads to a calcium concentrations 1,000 to 10,000 times higher than those found in normal cells (50). This increased calcium concentration then reacts with the high phosphorous concentrations found in cellular membranes, forming calcium phosphate and crystal growth (46, 48). A hypothetical model for calcification along with a calcified bioprosthetic valve can be seen in Figure 1.5.2. These processes are accelerated when combined with other factors, including mechanical stress, young patient age, kidney disease, diabetes, smoking, and immunological response (50, 51, 52, 53).
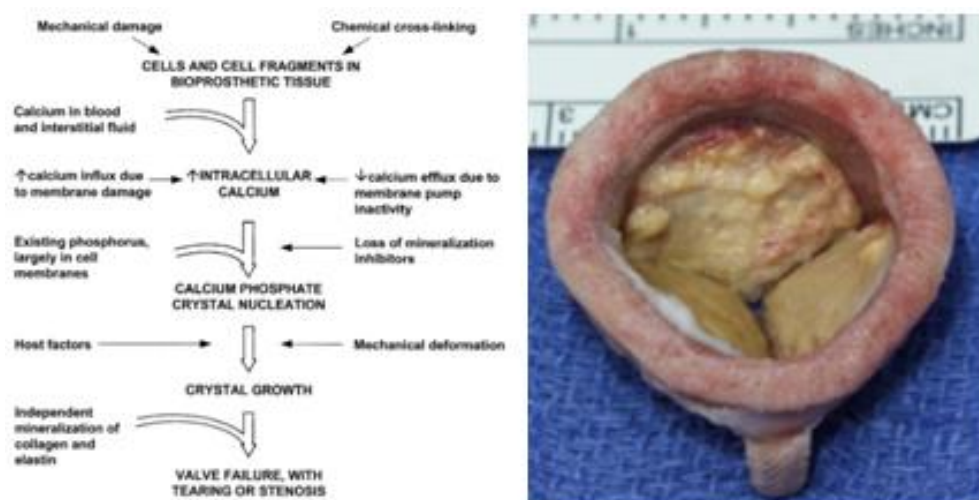

Figure 1.5.2 Extended hypothetical model for the calcification of bioprosthetic tissue (Left) (Figure taken from Ref. 54). Calcified bioprosthetic valve (Right) (Figure taken from Ref. 55)

Calcification has led to valve failure in every type of commercially available bioprosthetic valve including the Ionescu-Shiley Standard, the Ionescu-Shiley Low Profile, the Hancock Pericardial, the Carpentier Edwards Perimount, and the Mitroflow Pericardial Valve to name a few (46). Because of its major role in valve failure, calcification prevention and regulation are active areas of research.

Immunological response has been found to be a major factor in valve calcification (52, 53, 55). Bovine and porcine tissue both express α-Gal epitopes, surface molecules that cause an immune response when implanted in humans. Mice studies with anti-α-Gal antibodies expressed an increased acute and chronic humoral immune response compared to those without anti-α-Gal antibodies. This corresponded with higher calcium levels and increased valve calcification (55). Due to its role in calcification, concentrations of immune system regulatory proteins were measured in HVD patients to determine if any could be used as indicators for valve calcification. Low serum levels of IL-8, a protein responsible for chemotaxis and neutrophil adhesion, were found to correlate with valve calcification (52). These studies suggest that valves causing decreased immune inflammation will increase the durability and patient safety.

Recent studies have also found that calcification can be caused by dysfunctional phosphocalcific metabolism, leading to a disruption in calcium-phosphate homeostasis (52, 53). Due to these findings, many studies have been carried out to determine phosphocalcific metabolism biochemical concentrations that indicate a propensity for bioprosthetic valve calcification. Osteoprotegrin and osteopontin deficiencies and

11

higher calcium-phosphorus product were associated with valve calcification (52, 53).

Vitamin D supplementation, calcium supplementation, and bisphosphonate use, are indirectly associated with valve calcification by causing an increase calcium-phosphorus product (50, 53, 56).

Using these concentrations as potential signs of valve calcification, patients at elevated risk should be monitored more closely and preventative steps should be taken to reduce the risk of device failure. Although previously stated criteria have been shown to correlate with valve calcification, none have been shown to directly cause it (52). Using a new imaging technique developed by Meuris *et al.,* physicians can detect progression of valve calcification, non-invasively, using a multislice CT scanning technique. The results of which can be used for quantification and evaluation of valve calcification (57).

Devitalization of cells caused by glutaraldehyde is another main source of valve calcification. Many different fixatives have been investigated as a replacement for/additive to glutaraldehyde, including cyanimide, 1-ethyl-3(-3 dimethylaminopropyl) carbodiimide hydrochloride (EDC), adipyl dichloride, hexamethylene diisocyanate (HMDC), glycerol and alginate azide. However, each novel fixative has its own advantages and disadvantages that have prevented their use as cross-linking reagents (58). Quercetin, a newer fixative, however, was shown to outperform glutaraldehyde as a cross-linking reagent. Quercetin cross-linked valves produced a soft valve matrix, increased ultimate tensile strength, increased thermal denaturation temperature, resisted enzymatic degradation, was 100 times less toxic than glutaraldehyde, and had an anticalcification effect on valve tissue (58). GLX

tissue treatment, another new approach used for reducing calcification, uses a combination of glutaraldehyde, formaldehyde-ethanol-Tween 80 solution, functional group capping, reducing Schiff base sites, sterilization, and glycerolisation. Capping the valves functional groups and reducing its remaining Schiff bases reduces the number of binding sites available for calcium, phosphates, and immunogenic factors. Treating the valve tissue with glycerolisation inhibits valve oxidation, preserving the valves collagen matrix (59). Patients treated with GLX processed valves showed a 93% reduction in calcium content compared to normally processed valves after 35 days (59). Long-term characteristics of this valve treatment method need to be studied more thoroughly, however, before it can replace the use of glutaraldehyde.

1.6 FDA Valve Requirements

The U.S. Food and Drug Administration (FDA) require that artificial heart valves undergo *in vitro* testing prior to approval for medical use. During *in vitro* testing, mechanical heart valves must undergo 600 million opening and closing cycles and prosthetic heart valves must undergo 200 million opening and closing cycles. For a physiological heart rate, this equates to 15 years and 5 years, respectively. The heart valve must fully open and fully close during each one of the cycles, and the average transvalvular pressure must be a minimum of 100 mmHg during valve closure (60, 61).

1.7 Accelerated Wear Testers

Heart valve durability is a major issue when designing both mechanical and bioprosthetic heart valves. Accelerated wear testers (AWTs) are used to test the mechanical properties of artificial heart valves, specifically, their durability, over a relatively short period of

time (62). Because of an AWT's ability to operate between 600 and 1000 beats per minute

(BPM), it is able to test the valve's mechanical properties over the valve's entire lifespan in just

1-2 years' time (60). Results from testing valves in AWTs have been comparable to results *in*

vivo. Valves that fail mechanically in AWTs have been shown to fail *in vivo* as well, when they

fail in AWTs, they have been shown to fail in the same way as they do *in vivo*, and the valves

that last longer in AWTs, also last longer *in vivo* (60). The use of AWTs has allowed researchers

to discover long-term issues in valves, with no risk to the patient lives, leading to improved

designs and better patient outcomes. Many commercial AWTs use an electromagnetic motor

to drive fluid through the valve in a closed loop system and often come with 6 independent

chambers as seen in Figure 1.7.1 (63, 64). The chambers can be used to test the same valve at

different physiologic conditions (stroke volume, heart rate, blood pressure, etc.) investigating

how even slight physiologic differences can affect valve performance. The chambers can also

be used to test many different valves using the same parameters, comparing novel valves to

clinically proven valves.

Figure 1.7.1 Commercially available AWT (Figure taken from Ref. 63)

1.8 Previous Studies

The fluid mechanics that determine valvular function are closely tied to the mechanical properties of the valve. Therefore, there have been many studies pertaining to the mechanical properties of implanted heart valves. Yoganathan *et al.* conducted a comprehensive study of ball and cage valves, tilting disk valves, bileaflet valves, and bioprosthetic valves that have been developed over the past 40 years comparing their fluid dynamic performances. Due to the variability in valve mechanical features, each valve had advantages and disadvantages when comparing flow velocities, EOA, regurgitant flow, and turbulent shear stresses. He concluded that there are still improvements needed in the development of artificial heart valves, specifically in terms of hemodynamic characteristics, thromboresistance, and bioprosthetic valve durability (65).

To improve upon these characteristics, Mol *et al*. tried to mimic the mechanical properties of native heart valves by creating a tissue engineered valve. They tried to create acellular allograft valve leaflets, thus removing detrimental immunological responses from the host and allowing recellularization and revascularization. Although promising, they found that there is a large infectious risk when using materials derived from animal valves. They also found that newly developed cells on the graft were unable to cope with the high mechanical loading that is characteristic of the host's heartbeat (66).

Rather than experimentally test artificial heart valves, another study conducted in 2007 decided to model them computationally. Using advanced computational fluid dynamic solvers, they were able to validate a three dimensional large scale flow field within a bileaflet heart valve. Although this is a large stride forward, a large scale flow field is only a small piece of the

overall valve mechanics. Studies must also be done on the small scale flow field and on both small and large scale flow fields simultaneously to fully understand how valve mechanics and fluid mechanics impact one another (67).

A study conducted in 2001 by Iyengar *et al*. experimentally tracked leaflet motion under pulsatile flow conditions using a novel imaging technique. To obtain the data, the investigators used a diode laser to project a 19x19 dot matrix onto the leaflet. They then used two boroscopes mounted with high speed cameras to capture unobstructed views of the leaflet motion from two different angles. Then using a flow loop and an imaging program, they were able to capture images at exact time points in which the velocity and pressure fields of the loop were also known (15). This data was then processed and used to create leaflet images at those time points along the cardiac cycle. This system is able to tie the mechanical movement of the valve with the fluid mechanics of the flow loop and can be used to study basic heart valve mechanics, valvular related diseases, and artificial heart valve issues *in vitro* that have been seen clinically.

1.9 Current Study

The aim of this study is to design an AWT using SolidWorks that will be compatible with the use of particle image velocimetry (PIV) and a high speed camera. The basic design consists of a driving motor, two flow chambers, a liquid reservoir, and an overall housing to hold all of the components. Simulations were carried out using COMSOL and SolidWorks to determine the fluid dynamic impact on the stresses experienced by the AWT's flow chambers. The mechanical stresses were then used to determine if the AWT would be able to withstand testing of the bioprosthetic valve for the FDA required number of cycles. The stresses on the valve were also

compared to results seen clinically. By creating an AWT that is compatible with PIV

measurements, the flow field and structural integrity of a bioprosthetic heart valve can be

studied over its entire lifespan *in vitro*, giving insights into valve degradation mechanisms and

their impact on valve performance.

Chapter 2

Methods

2.1 Particle Image Velocimetry

The design of the AWT must be compatible with a PIV system. Therefore, a brief theory

of PIV will be discussed herein.

PIV provides a non-invasive way to determine the velocity measurements within a flow

field along different planar locations. By taking measurements along many planes in both the

normal and parallel planes, PIV can reconstruct a three dimensional flow field. A typical

diagram of a PIV setup can be seen in Figure 2.1.1.
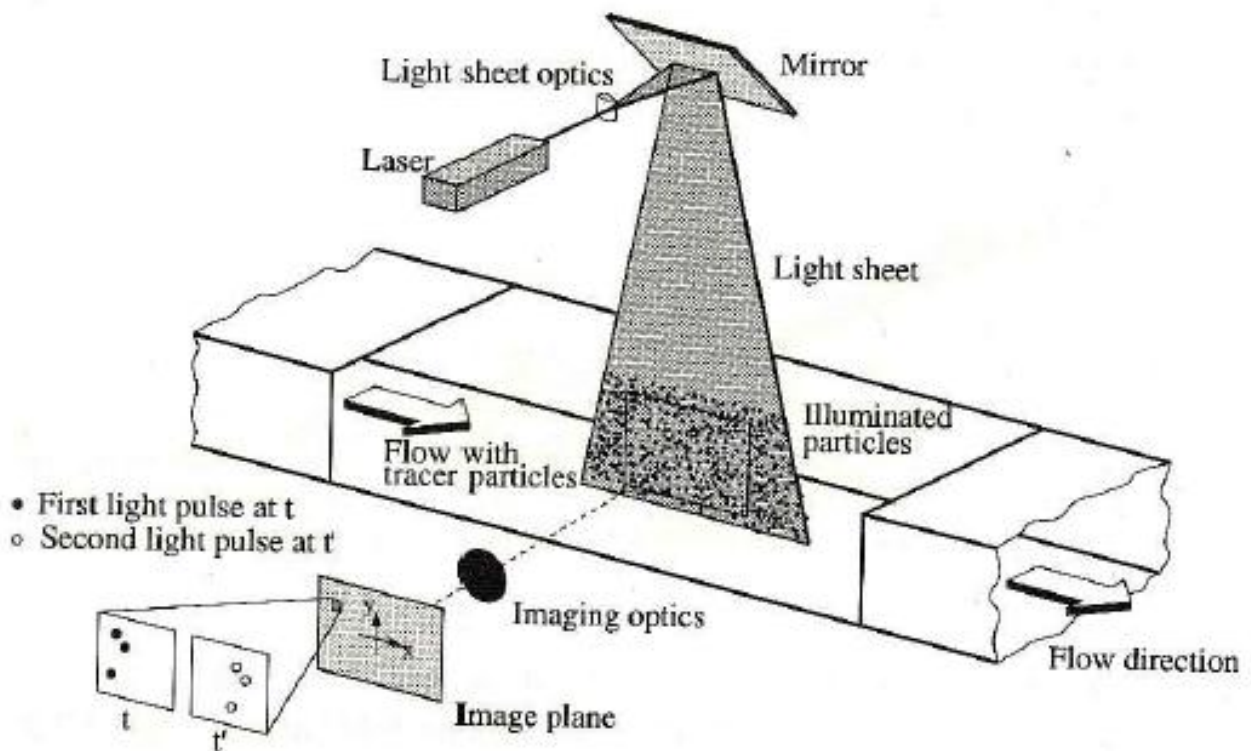
Figure 2.1.1 Diagram of typical PIV experimental design (Figure taken from Ref. 68)

To determine the flow velocity, a PIV system takes two images at times, Δt, apart from each other as denoted in Figure 2.1.1 by the t and t' image frames. The fluid contains hollow glass spheres that are captured in each image frame by a charge-coupled device (CCD) camera. To determine the velocity, the images must be divided into small interrogation regions (IRs) during post processing. The average motion of all of the particles within each IR is determined using cross correlation. This calculation is used to create a displacement vector, which is then divided over Δt to determine the velocity of the fluid in the IR. A velocity field for each plane can be obtained by carrying out this process over every IR in the plane (69).

To permit image acquisition along the plane of interest, both the flow chamber and the fluid must be transparent. When using PIV to study the cardiovascular system, Non-Newtonian blood analogs can be used to mimic the shear thinning viscoelastic properties that blood exhibits. It is also beneficial to use a fluid with a refractive index matching that of the flow chamber. This minimizes optical distortion of the light sheet when passing between the solid-fluid boundary allowing for accurate PIV measurements.

As an example, PIV images can be acquired using the Phantom Miro M-Series (VisionResearch) CCD camera with a resolution of 1920x1080 at 1500 fps. Focusing lenses, such as the Zeiss Otus 1.4/55mm lens are often used to provide a better resolution on the region of interest. Illuminating the particles in the flow field can be accomplished by using one of many commercially available dual laser pulsed PIV systems (TSI Inc., St. Paul, MN, U.S.A.). The pulsed lasers pass through a cylindrical lens and a spherical focusing lens that convert the beams into pulsed light sheets. The camera is oriented so that it is perpendicular to the light sheet created

by the laser, which can be seen in Figure 2.1.2, allowing the camera to track the particles that are illuminated in the light sheet's plane.
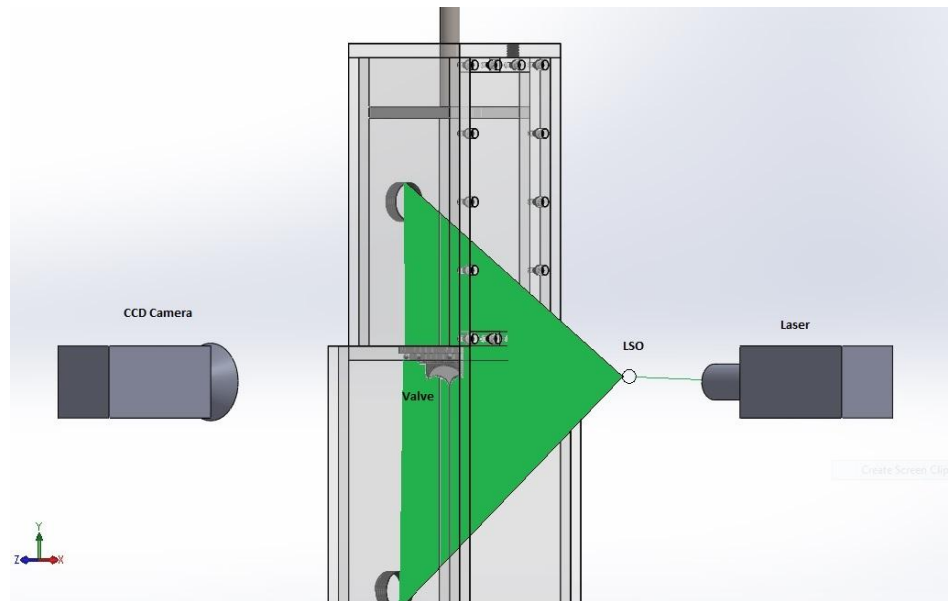
Figure 2.1.2 PIV setup for studying fluid flow through the valve of interest.

2.2 SolidWorks Design

Using SolidWorks 2014-2015 (SolidWorks Corp., 2014), an AWT was designed for a bioprosthetic heart valve that is compatible with a PIV system similar to the one described in the previous section. To achieve this, the design required a flow chamber with flat surfaces. It also needed to be transparent. The original design was composed of two identical flow chambers attached to a flow loop and a liquid reservoir. This design relied on a large liquid reservoir to create the needed 100 mmHg transvalvular pressure gradient during valve closure and only used the driving motor to open the valve. This design had to be modified, however, to reduce the total liquid volume needed for the system. A better way of bonding the two flow chambers to each other needed to be devised as well. The new design that was created relied

on the motor to create the required pressure gradients, allowing the liquid reservoir's size to be reduced significantly. Based off of the motor's torque output, the chamber and piston head dimensions were modified. Chamber 2's size was also increased to hold part of Chamber 1 inside of it. This allowed for a stronger, more durable bond between the two chambers. The chambers and motor were then attached to a small overall housing to hold everything in place and reduce any vibrations caused by the motor's rotation rate. The design again had to be modified when incorporating the PIV system into the AWT setup. Different CCD cameras have different focusing distances and to accommodate for the variability, the overall housing had to be redesigned. The new housing elevated the AWT system off of the ground to make room for the CCD camera. Chamber 1 was also modified during this design revision, creating an opening in the chamber wall to allow access to the valve being studied. More minor modifications were made as well including a countercurrent heat exchanger in the liquid reservoir to reduce the potential for thermal variables, an air cap on Chamber 1 to remove unwanted air bubbles, and a drainage tube in Chamber 2 to empty the AWT when not in use. The final design can be seen in Figure 2.2.1. The motor used for the AWT was the 10J151 Motor from Dayton Electric Mfg. Co., which is rated at 1000 RPM. This rotation rate will meet both the 600 and 200 million cycles required by the FDA for mechanical and bioprosthetic valves, respectively within one year's time. When loaded, this motor is rated to produce 0.65 Nm of torque. A piston head of 79.06 mm x 79.06 mm was used to create a pressure gradient of 120 mmHg. The piston head is attached to the driving motor via 5 parts that translate the motor's rotational motion into linear motion and can be seen in Figure 2.2.2.
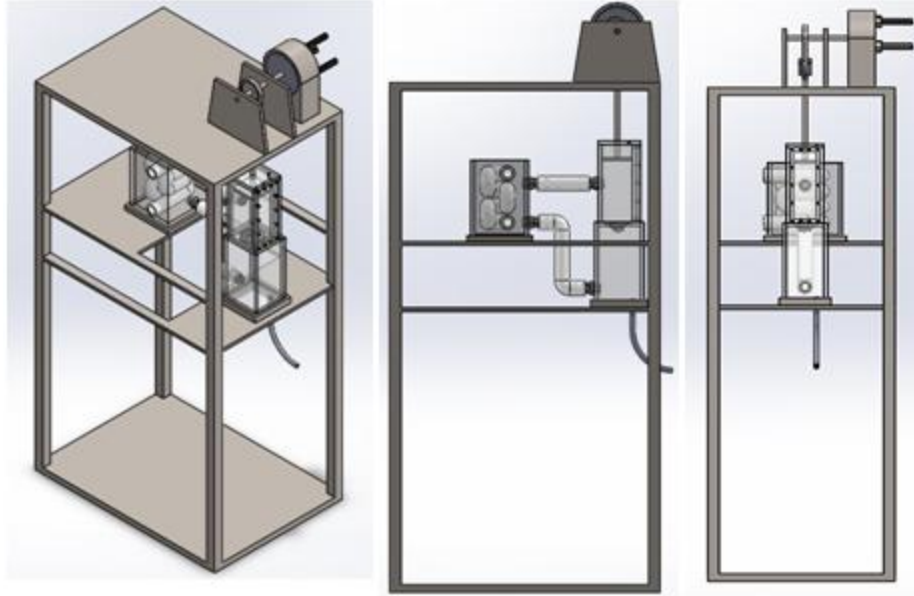
Figure 2.2.1 Accelerated wear tester. Isometric view (Left). Front view (Middle). Side view (Right)
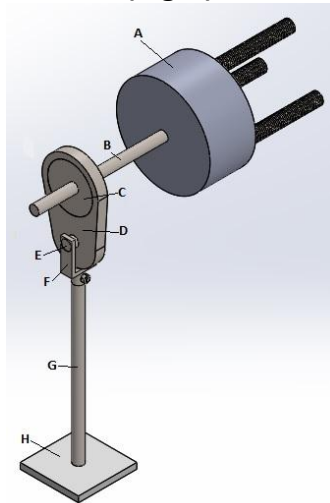
Figure 2.2.2 Motor and piston setup. A, Motor; B, Piston Shaft; C, Piston translation part; D, Piston translation part; E, Piston translation part; F, Piston translation part; G, Piston translation part; H, Piston head

The piston head is placed inside two cube flow chambers attached to a flow loop shown in Figure 2.2.3. Chamber 1 contains a one way valve, the piston head, an air cap, an interchangeable valve slot, and the valve to be studied using PIV. Chamber 2 contains a drainage tube and an outflow tube. The chambers are air and liquid tight so that no leakage

22

occurs. This is achieved through the use of gaskets and acrylic bonding agents. The piston head

drives the fluid through the flow chambers and flow loop by creating a pressure gradient. The

one way valve allows flow into Chamber 1 during the piston's up-stroke and prevents reverse

flow from occurring during the piston's down-stroke. The air cap allows for the removal of air

bubbles in the flow loop prior to starting the AWT. The interchangeable valve slot can be used

for attaching different types of valves. The drainage tube is used for emptying the flow

chambers and flow loop when the AWT is not in use.
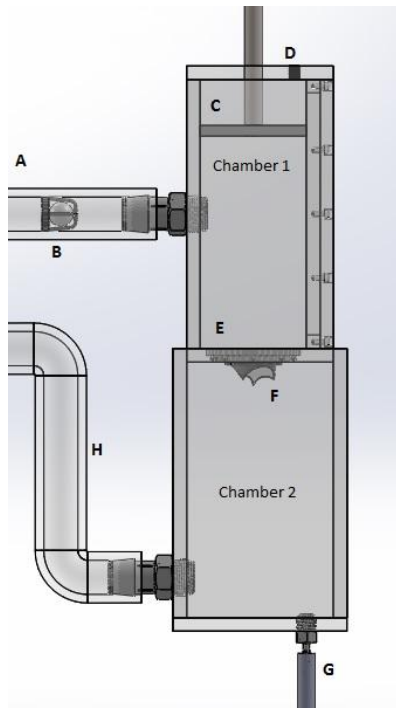
Figure 2.2.3 AWT setup. A, Inflow pipe; B, One-way inlet valve; C, Piston; D, Air bubble cap; E, Interchangeable valve slot; F, Valve to be studied; G, Drainage tube; H, Outflow pipe

The two chambers are attached to a liquid reservoir, via the inlet and outlet tube. The

liquid reservoir is used to fill the flow loop and the flow chambers with fluid up to the piston

head's surface. The liquid reservoir also has a countercurrent heat exchanger in it, which allows

the liquid to be maintained at a specific temperature for the duration of the experiment.   This

can be seen in Figure 2.2.4. Maintaining a constant temperature keeps the viscosity of the

liquid constant. It also removes any thermal effects that temperature changes can have on

fluid flow.
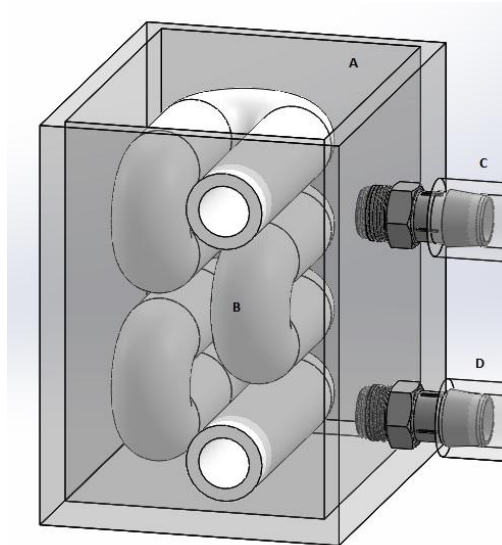
**Figure 2.2.4 Liquid housing setup. A, Liquid reservoir; B, Countercurrent heat exchanger;
C, Chamber inflow; D, Chamber outflow**

The AWT housing is designed to keep each part in place and reduce the vibration caused

by the quick rotation of the motor. Fixing the AWT in place is crucial for accurate PIV

measurements. The overall housing also elevates the AWT system off the ground, which

accommodates the large focusing distance of the CCD camera and focusing lens used for the

PIV setup.

A valve that consists of three leaflets and a protective housing was created to model a

bioprosthetic aortic valve and can be seen in Figure 2.2.5. The valve leaflets were modeled in

SolidWorks as a plastic with mechanical properties mimicking those of current bioprosthetic

valves. These can be found in Table 2.2.1 (70, 71). The elastic modulus of bovine pericardium is

not constant, but can be modeled as a power approximation fitted to experimental data found

by Noort *et al*. and can be seen in Figure 2.2.6 (72). Component materials and material

properties can be found in Appendix A.
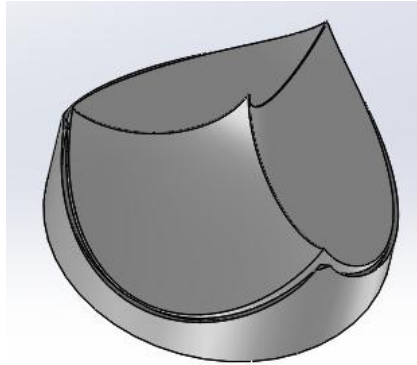
Figure 2.2.5 Bioprosthetic aortic heart valve

Table 2.2.1 Material properties of a bioprosthetic heart valve (70, 71, 72)

Component	Material	Young's Modulus (N/mm^2)	Poisson's Ratio	Mass Density (kg/m^3)
Valve Leaflets	Bioprosthetic	See Figure 2.2.6	0.45	1070
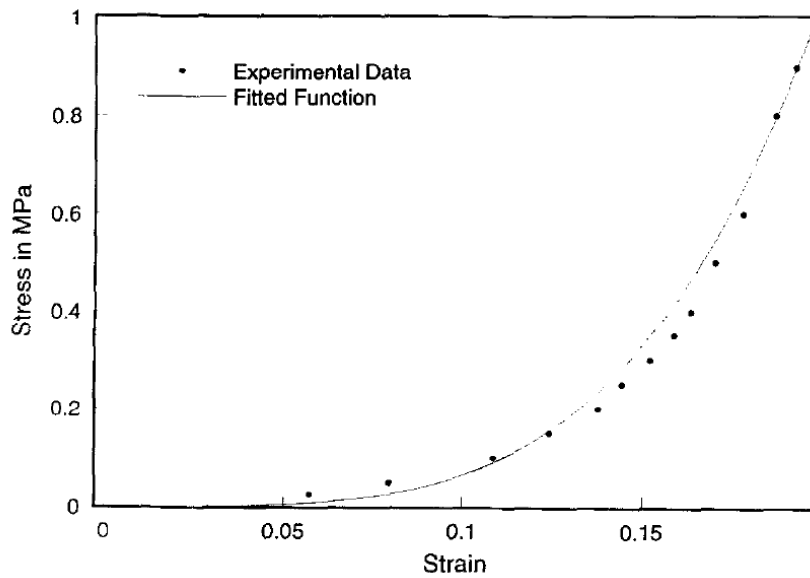
Figure 2.2.6 Experimental stress strain data for a bovine pericardium by Noort et al. fitted with a power approximation (Figure taken from Ref. 72)

25

2.3 Simulations

Simulations were performed using both COMSOL and SolidWorks to determine the feasibility of the AWT design that was created. The validation process is shown in Figure 2.3.1.
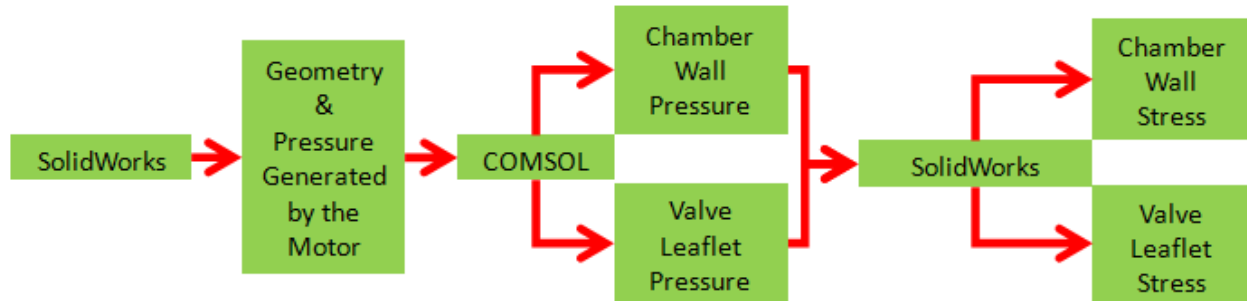
Figure 2.3.1 AWT design validation process.

Each simulation was first carried out using a medium sized mesh. To ensure that the result was not mesh sensitive, the simulation was rerun using both a smaller and larger mesh size. After confirming the simulation's result was accurate, the value acquired from the medium sized mesh was used for each subsequent simulation.

The first simulations performed were fluid-structure interaction (FSI) models. A simplified two dimensional model of the AWT chambers and valve was created in COMSOL Mutliphysics 2015 (COMSOL Inc. 2015). The geometry of the model was based on the initial SolidWorks design and was assumed to be symmetrical along the z-axis. The first simulation run, modeled the piston's up-stroke. During this time, the valve is assumed to be closed, so only the inlet and Chamber 1 were taken into consideration as seen in Figure 2.3.2. The simulation parameters can be seen in Table 2.3.1. The inlet was 10 mm x 100 mm long and Chamber 1 was 200 mm x 79.06 mm. An inlet gauge pressure of 0 mmHg was used to simulate the fluid entering the chamber and a gauge pressure of -120 mmHg at the top of the chamber

was used to simulate the suction created by the motor's movement. The study was run with a maximum time step of 0.01 s from 0 s to 19.37 s allowing the simulation to reach a steady state flow. The solver was run using the arbitrary Lagrangian-Eulerian (ALE) technique. This technique allows the solver to simultaneously solve for a deforming geometry and a changing flow field that is caused by the deforming geometry. The flow was solved using the incompressible Navier-Stokes equations, Equation 2.3.1, for a velocity field and pressure in a moving coordinate system and the incompressible continuity equation, Equation 2.3.2:

$$\rho\frac{\partial \boldsymbol{u}}{\partial t} - \nabla \cdot [-pI + \eta(\nabla \boldsymbol{u} + (\nabla \boldsymbol{u})^T)] + \rho\big((\boldsymbol{u} - \boldsymbol{u}_m) \cdot \nabla\big)\boldsymbol{u} = F \qquad (2.3.1)$$

$$\nabla \cdot \boldsymbol{u} = 0 \qquad\qquad (2.3.2)$$

Where $\boldsymbol{u}$= (u, v) is the velocity field, p is the pressure, I is the unit diagonal matrix, F is the volume force affecting the fluid, η is dynamic viscosity, ρ is the density, $(\nabla \boldsymbol{u})^T$ is the transverse matrix of divergence of $\boldsymbol{u}$, and $\boldsymbol{u}_m$= (u_m, vm) is the coordinate system velocity. The structural deformation is solved for by summing the pressures and viscous forces that the valve boundary is exposed to by the fluid:

$$F_T = -n \cdot (-pI + \eta(\nabla \boldsymbol{u} + (\nabla \boldsymbol{u})^T)) \qquad (2.3.3)$$

Where n is the vector normal to the valve boundary. These equations are then solved on a freely moving deformed mesh. Winslow smoothing is used to calculate the mesh's deformation compared to its initial shape. Once finished, the solver stores the fluid velocity throughout the chamber, and the pressure values that the chamber experienced. The pressure value seen at the closed valve was used to determine the necessary hydrostatic pressure in Chamber 2 to achieve a minimum average transvalvular pressure of 100 mmHg at closure.

Another FSI simulation was run to model the motor's down-stroke. Due to the fact that the valve opens during the down-stroke of the piston, both chambers, along with the valve had to be modeled. The alternate geometry and parameters can be seen in Figure 2.3.3 and Table 2.3.2, respectively. Again, the geometries for the components are based off of the initial SolidWorks design. The fluid flows from the inlet (marked in Figure 2.3.3) into Chamber 1. The flow then passes through the valve into Chamber 2 and then into the outlet (also marked in Figure 2.3.3).
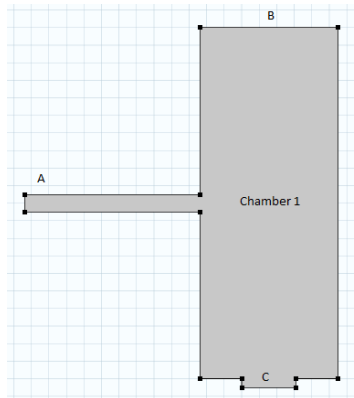

Figure 2.3.2 Motor up-stroke simulation geometry. A, Inlet; B, Motor pressure; C, Closed valve
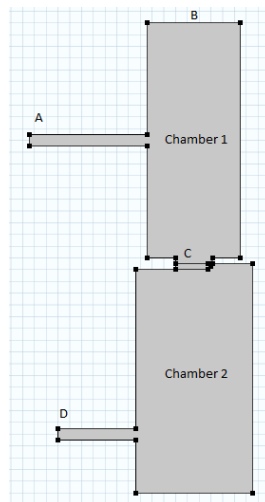

Figure 2.3.3 Maximum pressure simulation COMSOL setup. A, Inflow; B, Motor Pressure; C, Valve; D, Outflow

Table 2.3.1 Simulation of motor up-stroke parameters

Inlet (Pa)	0
Motor Pressure (Pa)	-15999*(1-EXP(-0.5*t))
Fluid Density (kg/m^3)	1000
Fluid Viscosity (Pa*s)	0.001
Time (s)	19.37

Table 2.3.2 Simulation of motor down-stroke parameters

Inlet (Pa)	0
Outlet (Pa)	15999*(1-EXP(-0.5*t))
Fluid Density (kg/m^3)	1000
Fluid Viscosity (Pa*s)	0.001
Solid Density (kg/m^3)	1070
Solid Young's Modulus (N/mm^2)	See Figure 2.2.6
Solid Poisson's Ratio	0.45
Time (s)	19.37

The inlet and Chamber 1 had the same geometries as the last simulation. A 5 mm x 30 mm valve was added to the bottom of Chamber 1. The geometry of the valve was simplified into a one leaflet valve, which differs from the three leaflet valve used in the AWT design; however, its material properties were the same. The valve allowed flow to pass into Chamber 2. Chamber 2 was 200 mm x 99.06 mm. Finally, the flow exited through the 10 mm x 66.07 mm outlet. A gauge pressure of 120 mmHg in Chamber 1 was used to simulate the pressure created by the motor head and a gauge pressure of 0 mmHg was used to simulate the hydrostatic pressure in Chamber 2. Chamber 2's pressure was calculated based on the previous simulation. The study was run with a maximum time step of 0.01 s from 0 s to 19.37 s allowing the simulation to reach a steady flow state. Again, the simulation was solved using the ALE technique. The corresponding values for this study were also stored.

Next, linear stress simulations were carried out on Chamber 1 and 2 using SolidWorks Simulation. Using the stored material properties in SolidWorks, each chamber was modeled as

an acrylic (high-medium impact) plastic. The inner walls of each chamber were then exposed to

the maximum pressures that were created by the motor's down-stroke. These pressures were

determined during the previous COMSOL simulations. The pressure was applied linearly over a

time period of 0.03 seconds at which point, the maximum pressure was reached. The solver

then stored the von Mises stresses along the surface of the chambers. Simulation parameters

and material properties can be seen in Table 2.3.3 and Table A.1, respectively.

The chambers were then exposed to the pressure values created during the piston's up-

stroke in the same manner as the previous study. Simulation parameters and material

properties can be seen in Table 2.3.4 and Table A.1, respectively. The solver then stored the

von Mises stresses along the surface of the chambers.

Finally, simulations were run on the bioprosthetic heart valve to determine if the

pressure gradients produced by the motor fully open and fully close the valve. The valve

material was programmed to have the material properties of a bioprosthetic heart valve that

were stated in the previous section. The valve leaflets were exposed to the pressures found

along the bottom surface of Chamber 1 during each set of COMSOL simulations. These

pressures correlated to pressure drops of -16,000 Pa and 18,000 Pa across the valve, which can

be seen in Table 2.3.5 and Table 2.3.6. The solver then stored the von Mises stress along the

valve surfaces. Material properties for the valve are listed in Table 2.2.1 and Table A.1.

Table 2.3.3 SolidWorks chamber wall stress test (Motor Down-Stroke) parameters

Chamber 1 Pressure (Pa)	18,000
Chamber 2 Pressure (Pa)	12,000
Time (s)	0.03

Table 2.3.4 SolidWorks chamber wall stress test (Motor Up-Stroke) parameters

Chamber 1 Pressure (Pa)	-16,200
Chamber 2 Pressure (Pa)	0
Time (s)	0.03

Table 2.3.5 SolidWorks valve leaflet stress test (Motor Down-Stroke) parameters

Leaflet Pressure (Pa)	18,000
Time (s)	0.03

Table 2.3.6 SolidWorks valve leaflet stress test (Motor Up-Stroke) parameters

Leaflet Pressure (Pa)	-16,000
Time (s)	0.03

Chapter 3

Results

3.1 COMSOL Simulations

Due to the fact that COMSOL does not handle either turbulent flow or large deformations very well, the pressure in Chamber 1 had to be decreased slowly over time until it reached an asymptotic value of -120 mmHg. This pressure difference can be seen in Figure 3.1.1. During the simulation, the pressure along the walls of the chamber were calculated. Because the magnitude of the pressure asymptotically approaches -120 mmHg, the velocity of the flow field and the pressures along the chamber walls slowly change as well. The fluid is sucked in by the negative pressure gradient and hits the wall of the chamber. The flow then separates and forms vortices below the inlet and above the inlet. The magnitude of the vortices above the inlet are smaller than those below the inlet. Once developed, the flow direction remains constant, while the magnitude of the velocity increases over time until it reaches a maximum value at 19.37 s. This is also when the largest pressure gradient along the chamber walls occur. The minimum pressure experienced inside the chamber was -16,106.7 Pa, or -120.80 mmHg. This can be seen in Figure 3.1.1. This pressure was then rounded to -16,200 Pa, or -121.51 mmHg, and used in the following SolidWorks study. The minimum pressure at the valve surface was also measured and was found to be -16,000 Pa, or -120 mmHg. Because this value is smaller than -100 mmHg, the gauge pressure inside Chamber 2 did not need to be increased relative to Chamber 1.

The same process was carried out for the second COMSOL simulation, which modeled the pressures caused by the motor's down-stroke. Because the magnitude of the pressure asymptotically approaches 120 mmHg, the velocity of the flow field and the pressures along the chamber walls approach asymptotic values as well. The fluid is pushed through the valve by the pressure gradient caused by the piston head. The flow is directed by the valve and hits the wall of Chamber 2. It then hits the bottom of the chamber and forms a large vortex that encompasses the entirety of the chamber. During the vortical flow, the fluid is eventually able to pass into the outflow tube. The magnitude of the velocity of the fluid in the vortex slowly increases until it reaches a steady state at 19.37 s. The maximum pressure caused by this simulation occurred at 19.35 s and was 17,720 Pa, or 132.91 mmHg. This can be seen in Figure 3.1.2. The pressure is caused by a combination of the piston's down-stroke and the fluid flow caused by it. This pressure was then rounded to 18,000 Pa and was used in the subsequent SolidWorks simulation. The pressure in Chamber 2 during the piston's down-stroke was found to be 11,480 Pa and was rounded to 12,000 Pa for the SolidWorks simulation.
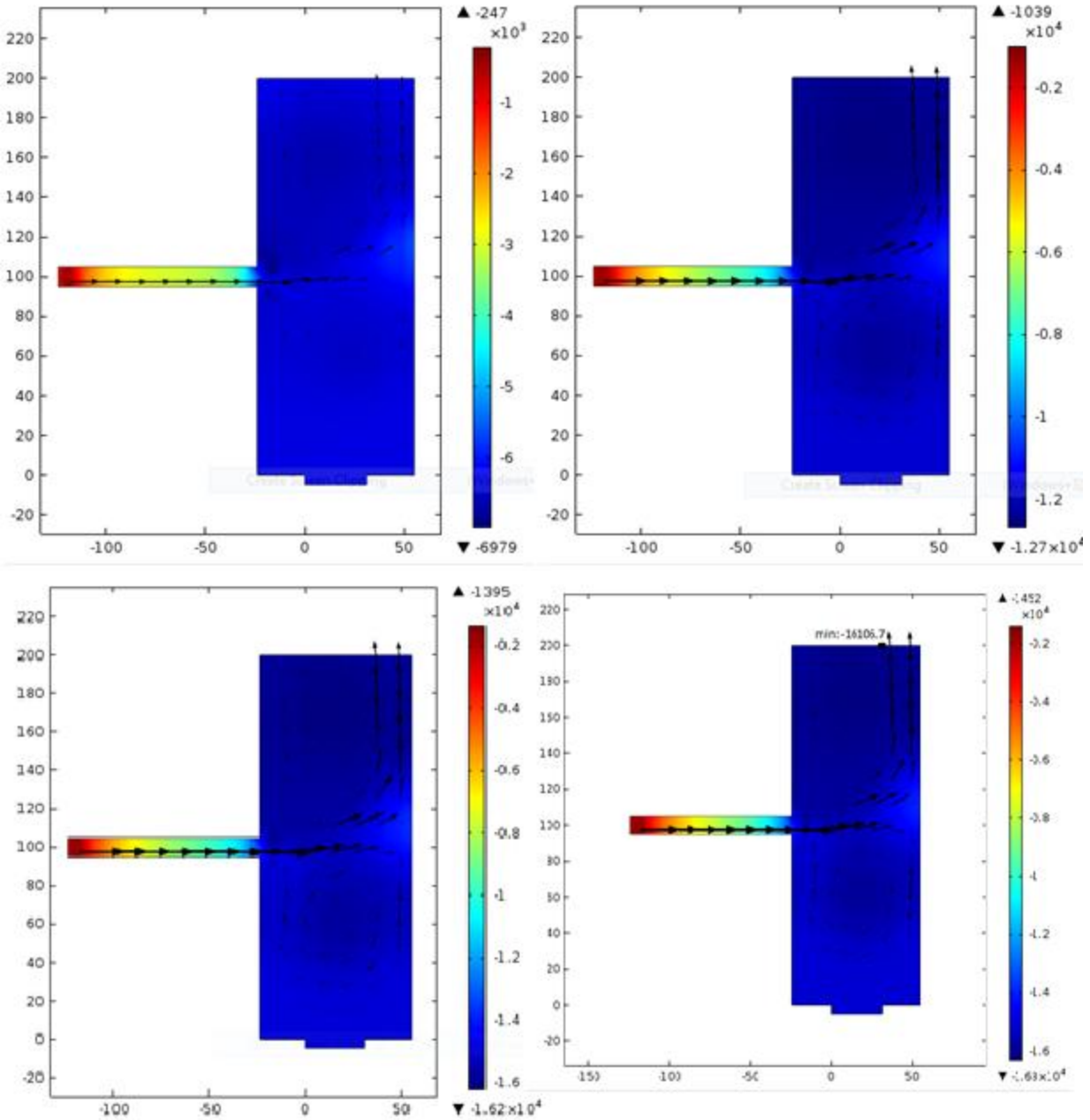
Figure 3.1.1 Minimum pressure at the chamber wall seen during the up-stroke of the motor with fluid velocity/direction at different time points during the cycle. 1 second (Top left); 3 seconds (Top right); 10 seconds (Bottom left); 19.37 seconds (Bottom right).
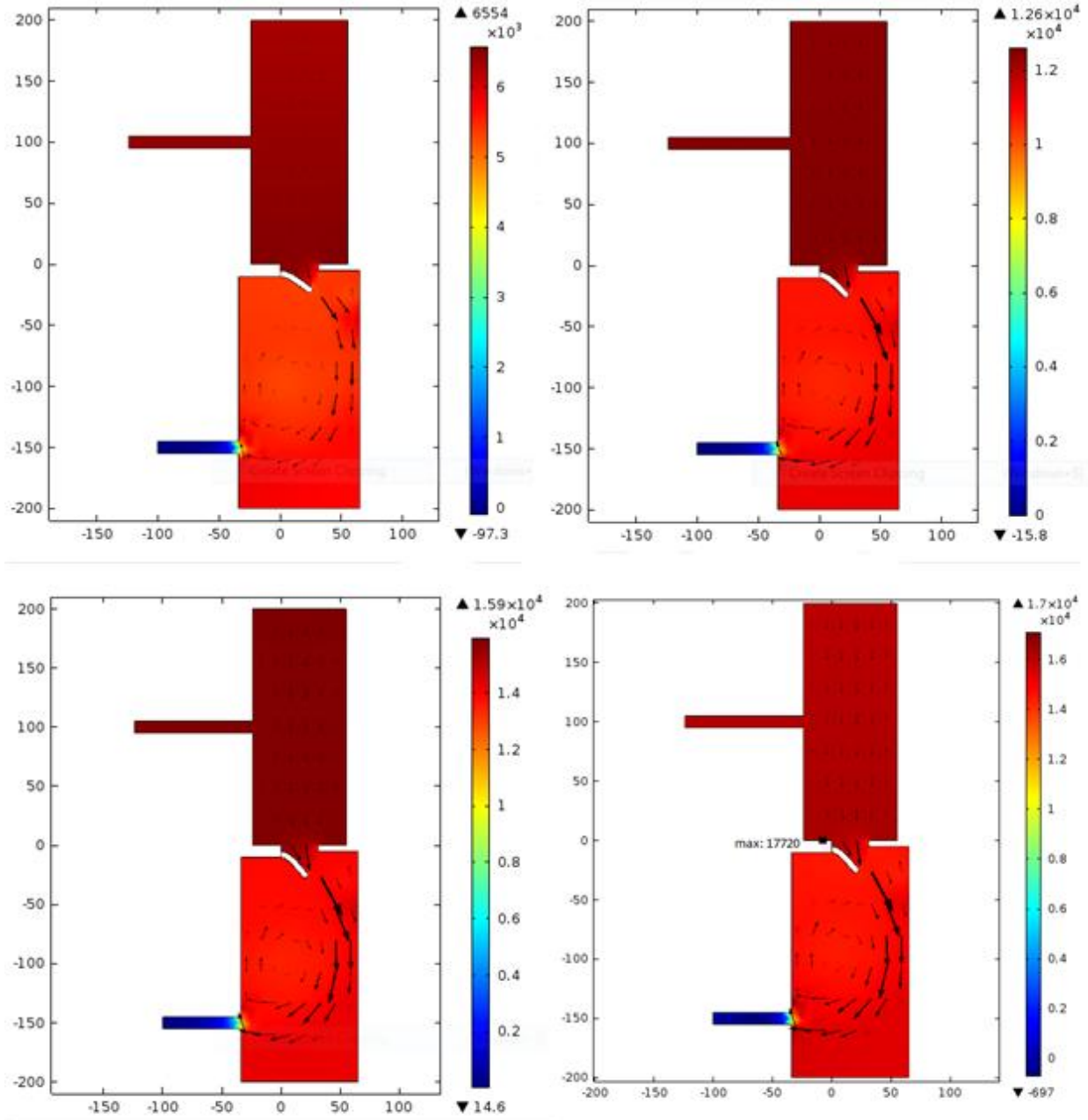
Figure 3.1.2 Maximum pressure at the chamber wall seen during the down-stroke of the motor with fluid velocity/direction at different time points during the cycle. The valve leaflet shown is deformed from its original geometry due to the fluid forces caused by the down-stroke of the motor. 1 second (Top left); 3 seconds (Top right); 10 seconds (Bottom left); 19.35 seconds (Bottom right).

3.2 SolidWorks Simulations

The first simulation run with SolidWorks determined the maximum stresses that the walls of the acrylic chambers experience during the piston's down-stroke. Chamber 1 had a pressure of 18,000 Pa placed on all of the walls and the top of the valve changing slot, while Chamber 2 had a pressure of 12,000 Pa placed on all of the walls, the bottom of Chamber 1, and the bottom of the valve changing slot. The stresses were plotted along the surface of the chambers. At 0.01 s, stresses begin to build along the inflow of Chamber 1 and the attachment areas of the Chamber 1 opening.   These stresses continually increase as the pressure builds over the 0.03 s. Stress concentrations can also be seen along the center of the walls of Chamber 1. A smaller stress concentration can be found at the outflow of Chamber 2. Finally, at 0.03 s when the maximum pressure is being applied to the chamber surfaces, the maximum stress of 0.99 MPa occurs at the attachments of the opening for Chamber 1. This progression can be seen in Figure 3.2.1.

The same simulation was run again; however, it was modified to use the pressures that occur during the motor's up-stroke. Chamber 1 had a pressure of -16,200 Pa placed on all of the walls and the top of the valve changing slot, while Chamber 2 did not have a pressure placed on any of the walls because the hydrostatic gauge pressure in Chamber 2 is 0 Pa. The stress progression during this simulation is very similar to that of the last one. At 0.01 s, stresses begin to build along the inflow of Chamber 1 and the attachment areas of the Chamber 1 opening.   These stresses continually increase as the pressure builds over the 0.03 s. Stress concentrations can also be seen along the center of Chamber 1's walls. Finally, at 0.03 s when the maximum pressure is being applied to the chamber surfaces, the maximum stress of 0.86

MPa occurs at the attachments of the opening for Chamber 1. This progression can be seen in Figure 3.2.2. The maximum stress that occurs during the up-stroke is approximately the same as the stress experienced during the motor's down-stroke.

Next, simulations were run on the valve leaflets to determine if the pressures generated during the piston's down-stroke can fully open them. A pressure of 18,000 Pa was applied to the bottom of the leaflets over an accelerated time period of 0.03 s. This pressure caused the valves to fully open. At 0.002 s, the valve fully opens with only 0.36 MPa of stress along its leaflets.   After it fully opens and the applied pressure continually increases, larger stresses begin to appear along the walls where the leaflets are attached. This can be seen after 0.01 s. These stresses begin to spread along the leaflet surface and finally reach a maximum stress of 2.06 MPa at 0.03 s. This progression can be seen in Figure 3.2.3.
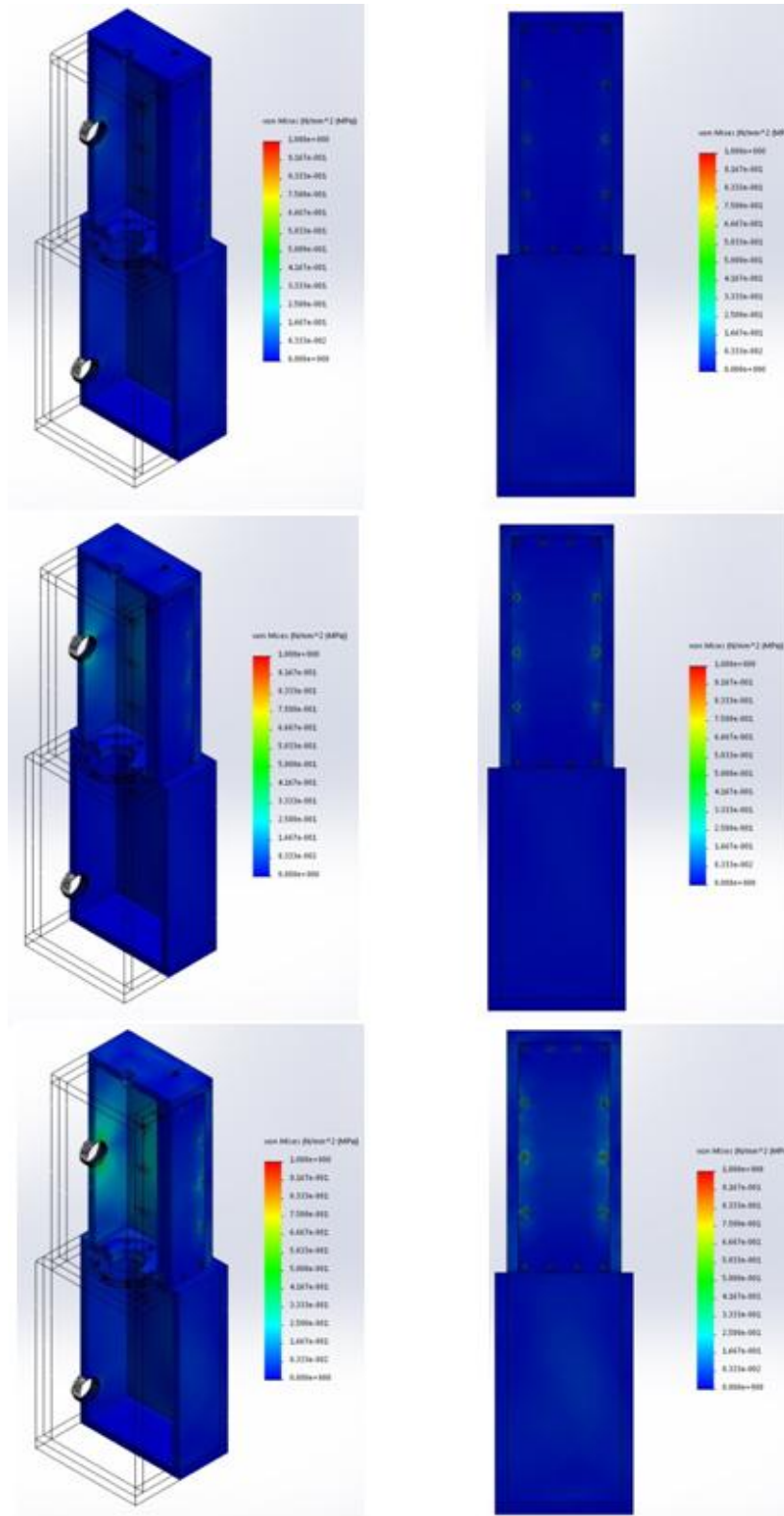
Figure 3.2.1 Chamber 1 & 2 von Mises stress due to piston's down-stroke. Isometric inside views (Left), Side views (Right). 0.01 s (Top); 0.02 s (Middle); 0.03 s (Bottom)
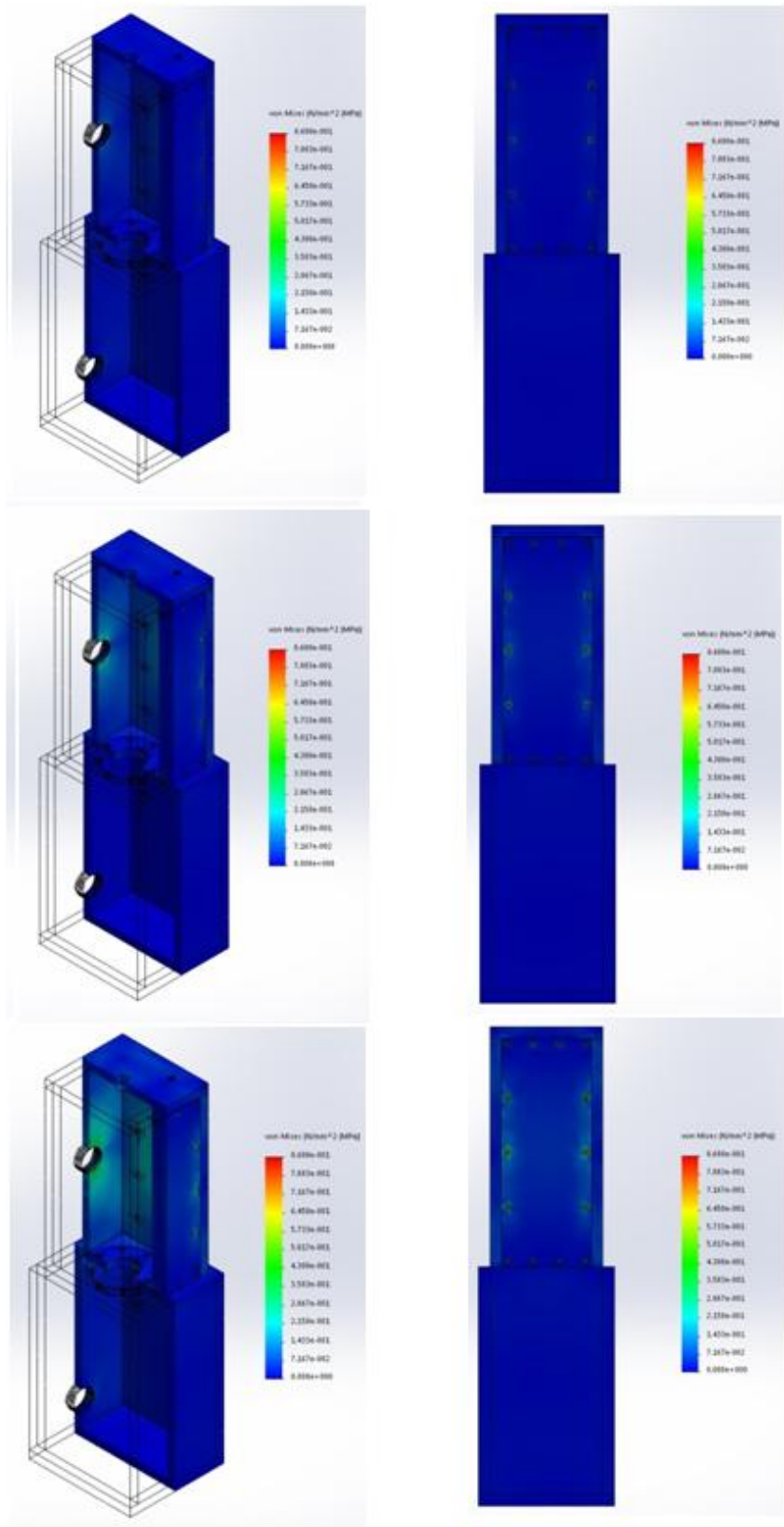
Figure 3.2.2 Chamber 1 & 2 von Mises stress due to piston's up-stroke. Isometric inside views (Left), Side views (Right). 0.01 s (Top); 0.02 s (Middle); 0.03 s (Bottom)

Finally, the same simulation was run on the valve leaflets again; however, the direction of the pressure gradient was changed and reduced to 16,000 Pa. Again, it was found that the pressure fully closed the valve.   At 3 x 10^{-4} s, the valve fully closes with 0.66 MPa of stress along its leaflets.   After it fully closes and the applied pressure continually increases, stresses begin to appear along the leaflet contact points. This can be seen after 0.01 s. These stresses begin to spread along the leaflet surfaces and finally reach a maximum pressure of 4.5 MPa at 0.03 s. This progression can be seen in Figure 3.2.4. The maximum von Mises stress experienced by the valve during either simulation was 4.5 MPa, with a maximum principal strain of 0.34 occurring during the piston's up-stroke and a maximum displacement of 16.6 mm occurring during the piston's down-stroke.
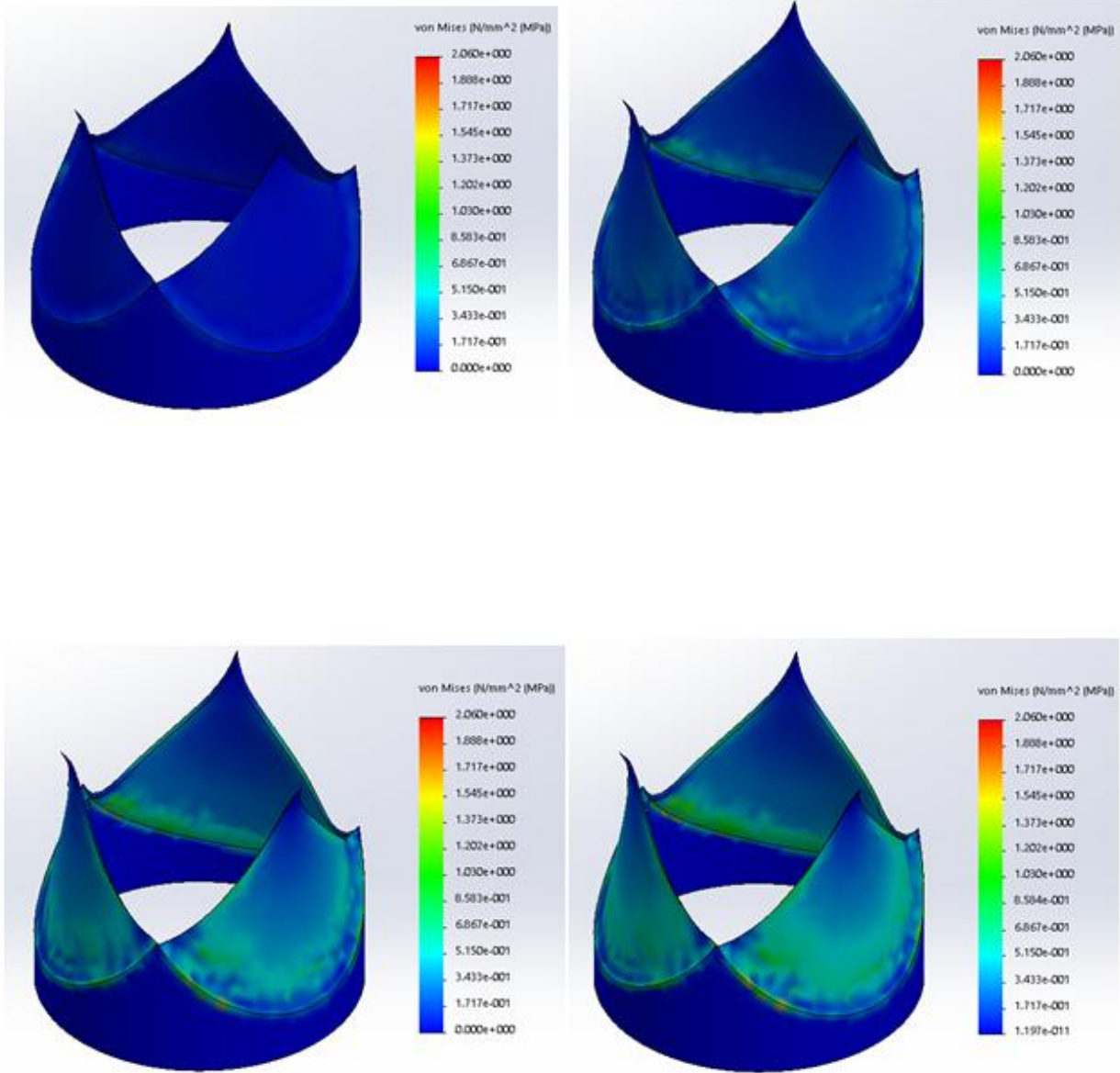
Figure 3.2.3 The development of stress along the valve during the piston's down-stroke. 0.001 s (Top left); 0.01 s (Top right); 0.02 s (Bottom left); 0.03 s (Bottom right).
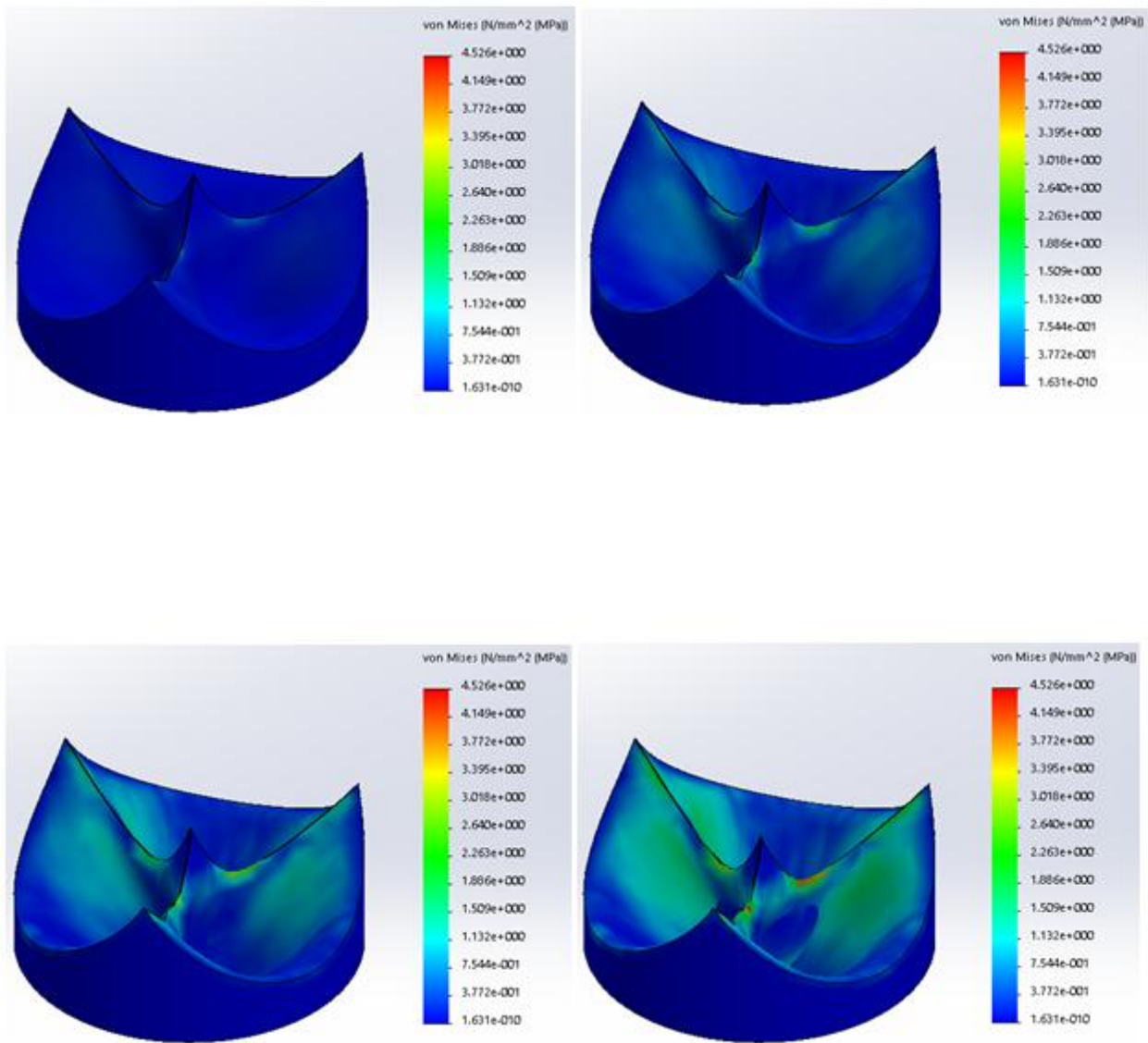
Figure 3.2.4 The development of stress along the valve during the piston's up-stroke. 3 x 10-4 s (Top left); 0.01 s (Top right); 0.02 s (Bottom left); 0.03 s (Bottom right).

Chapter 4

Discussion

4.1 Meeting FDA Requirements

For the design of the AWT to function properly, its flow chambers must be able to withstand the same number of loading and unloading cycles as the valve it is testing. The maximum stress that occurs on the chamber walls due to the fluid pressure created by the motor motion is 0.99 MPa. The fatigue life of extruded acrylic sheets is 38 MPa (73). This is a factor of 38 larger than the maximum stresses that the AWT chambers will experience. This means that the chambers should last indefinitely without cracking or breaking.

Another FDA requirement is that the bioprosthetic valve must always fully open and fully close during each cycle. As seen in the simulations, the bioprosthetic valve fully opens and fully closes during the piston's down-stroke and up-stroke, respectively. Therefore, when experiencing the pressure difference during both the down-stroke (ΔP = 135.01 mmHg) and the up-stroke of the motor shaft (ΔP = -120 mmHg) *in vitro,* the valve should fully open and fully close during each cycle.

Finally, during valve closure, the valve must have a minimum average transvalvular pressure of 100 mmHg. This pressure is achieved through a combination of the hydrostatic chamber pressure and the pressure created by the motor's up-stroke.

4.2 Valve Stresses & Deformation

During valve closure, the maximum stress experienced by the valve is 4.5 MPa. This is high compared to other findings. Martin and Sun exposed closed leaflets to peak pressures of 120 mmHg using a quasi-static loading technique. They recorded maximum valve stresses of

1.45 MPa (74). Li and Sun used the same pressure and loading technique and found maximum

valve stresses of 1.56 MPa (75). When Sabbah *et al.* incrementally increased the loading

pressure on closed valve leaflets from 0 mmHg to 120 mmHg; they recorded maximum stresses

of only 0.19-0.2 MPa (76, 77). This shows that load time plays a major factor in stress

calculations. Although the same amount of pressure was applied to the valve leaflets in all

three experiments, the pressure applied over a period of only 0.03 s created a much larger

stress on the leaflets compared to the pressure applied using the quasi-static or incremental

loading techniques. Increased stress values on the valve are one drawback to accelerated

testing.

As can be seen in Figure 3.2.3 and Figure 3.2.4, the valve undergoes very large

deformations. This is extremely relevant during valve closure. Leaflet geometry and leaflet to

leaflet contact plays a major role in closure mechanics. If the valve leaflets have deteriorated in

some way or are not symmetrical, like the ones that were modeled in the simulations, it can

greatly affect valve performance and cause regurgitant flow, increased leaflet stresses, or

inversion of the leaflets.

4.3 Simulation Limitations

The COMSOL simulations determined the pressure along the walls of the AWT flow

chambers. Although helpful, many assumptions were made during the study. First, the model

was simplified into two dimensions. This does not allow for the circular valve to be properly

modeled. Although the entire model was assumed to be symmetric about the z-axis, the

opening for the valve does not encompass the entire chamber. In reality, it ends before the

front and back edges of the chamber. The valve was also simplified into a single leaflet valve

rather than a three leaflet valve. This changes the direction of the flow as it passes through the

valve, deflecting it towards the chamber wall, rather than towards the bottom of the chamber.

Finally, the pressure magnitude was slowly increased rather than being applied

instantaneously. This created much more laminar flows rather than the turbulent flows that

would be seen in reality. The turbulence would affect the wall pressures along the chambers.

4.4 Accelerated Wear Tester & PIV Setup

Running a PIV study in concurrence with accelerated wear testing has never been done

before. A theoretical set up can be seen in Figure 4.4.1. This type of study will combine both

the motion of the valve and the motion of the fluid.
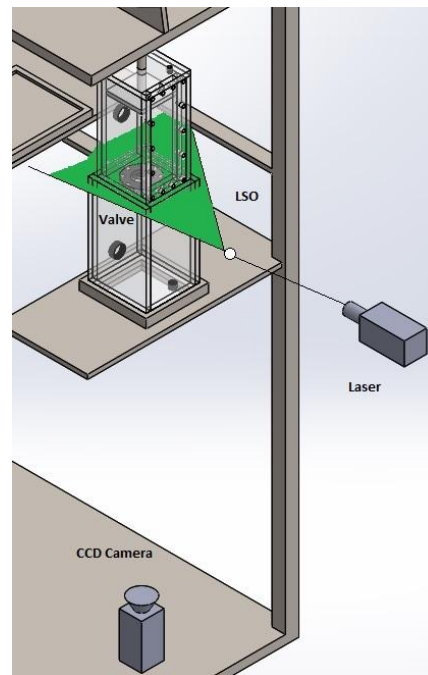
Figure 4.4.1 Theoretical AWT and PIV setup.

By combining both the solid mechanics and the fluid dynamics, this AWT with its PIV system can

be used to investigate how the flow fields of bioprosthetic heart valves are affected as the valve

deteriorates over time. This will give insights into possible areas of high shear rate, vortex

formation, areas of stagnation, areas of calcification, and sites at risk for thrombosis over the

entire lifespan of a bioprosthetic valve. Using this information, safer and more efficient heart

valves can be designed.

Chapter 5

Conclusions

5.1 Summary of Results

The most important result from this study was determining that the AWT would not break during the testing of the valve. The simulations showed that the maximum stress that either chamber experiences during a single rotation of the piston is 0.99 MPa. The fatigue strength of extruded acrylic sheets is 38 MPa, orders of magnitude higher than the maximum stress on the chamber walls. This shows that over the lifetime of the AWT, it will not crack or break regardless of the number of cycles it must endure. The 10J151 Motor from Dayton Electric Mfg. Co., is a continuous motor that is rated at 1000 RPM, that should theoretically be able to run for up to 3 years.

Second, it was shown that the valve will fully open and fully close during each cycle. Using the mechanical properties found in the literature for a bioprosthetic heart valve, it was found that the pressure drops across the valve created by the motor will fully open and fully close the valve.

Finally, it was shown that there is an average transvalvular pressure of 100 mmHg during valve closure. This was accomplished through a combination of the lower chamber's hydrostatic pressure and the negative pressure induced from the piston's up-stroke.

5.2 Future Studies

One avenue of further study would be to test different types of heart valves to make sure the pressure differences seen are enough to open and close each valve fully. This would

allow the AWT to be used with every kind of heart valve, greatly increasing its research

potential. Another avenue of future research is to physically build the AWT.   Due to the fact

that this study only designed the AWT, the next logical step would be to build it. This can be

accomplished by creating the components with the same measurements as the ones in the

SolidWorks design. The acrylic chambers need to be machined and then bonded together using

an acrylic bonding agent. The overall housing would also need to be machined. The piston

motor and high speed camera components needs to be bought and assembled. To record

accurate data, the PIV laser and CCD camera must be secured. The laser must also be able to

move from plane to plane to create the three dimensional flow field. Some type of system

needs to be developed prior to using the AWT for these components.

Appendix A

Component Material Properties

Table A.1 AWT components with corresponding materials and material properties

Component	Material	Youngs Modulus (N/mm^2)	Poisson's Ratio	Mass Density (kg/m^3)
Air Cap	Acrylic	3000	0.35	1200
Chamber 1	Acrylic	3000	0.35	1200
Chamber 1 Opening	Acrylic	3000	0.35	1200
Chamber 2	Acrylic	3000	0.35	1200
Piston	Alloy Steel	210000	0.28	7700
Piston Translation Part 1	Alloy Steel	210000	0.28	7700
Piston Translation Part 2	Alloy Steel	210000	0.28	7700
Piston Translation Part 3	Alloy Steel	210000	0.28	7700
Piston Translation Part 4	Alloy Steel	210000	0.28	7700
Piston Translation Part 5	Alloy Steel	210000	0.28	7700
Piston Shaft	Alloy Steel	210000	0.28	7700
Piston Head	PTFE	551	0.47	2320
Inflow Pipe	PVC	6	0.47	1290
Outflow Pipe	PVC	6	0.47	1290
Heat Exchanger	PVC	6	0.47	1290
Liquid Reservoir	PTFE	551	0.47	2320
0.5" Barb	PVC	6	0.47	1290
0.75" Barb	PVC	6	0.47	1290
Ball	PTFE	551	0.47	2320
Cage	PUR	2410	0.3897	1260
Drainage Tube	PVC	6	0.47	1290
Overall Housing	Alloy Steel	210000	0.28	7700
Valve Changing Slot	Silicon Rubber	5	0.394	1250
Sewing Ring	Polyurethane Foam Flexible	2.78	0.394	16.185
Valve Housing	PUR	2410	0.3897	1260
Valve Leaflets	Bioprosthetic	See Figure 2.2.6	0.45	1070

References

1. Roger VL, Go AS, Lloyd-Jones DM, Benjamin EJ, Berry JD, Borden WB, Bravata DM, et al. 2012. Heart disease and stroke statistics--2012 update: a report from the American Heart Association. *Circulation* 125(1):e2–e220.

2. *Explore Heart Valve Disease*. National Institute of Health, 16 Nov. 2011. Web. 16 Mar. 2015. <http://www.nhlbi.nih.gov/health/health-topics/topics/hvd>.

3. Mahmut, Ablajan, Marie-Chole Boulanger, Rihab Bouchareb, Fayez Hadji, and Patrick Mathieu. "Adenosine Derived from Ecto-Nucleotidases in Calcific Aortic Valve Disease Promotes Mineralization Through A2a Adenosine Receptor." *European Society of Cardiology* (2015): 1-12. *PubMed*. Web. 16 Mar. 2015.

4. Nkomo, Vuyisile T., Julius M. Gardin, Thomas N. Skelton, John S. Gottdiener, and Christopher G. Scott. "Burden of Valvular Heart Diseases: A Population-Based Study." *Lancet* 368 (2006): 1005-11. *PubMed*. Web. 9 July 2015.

5. Avadhani SA, Martin-Doyle W, Shaikh AY, Pape LA, Predictors of Ascending Aortic Dilation in Bicuspid Aortic Valve Disease - *a Five-Year Prospective Study*, *The American Journalof Medicine* (2015), doi: 10.1016/j.amjmed.2014.12.027.

6. Helms, Adam S., and David S. Bach. "Heart Valve Disease." *Prim Care Clin Office Pract* 40 (2013): 91-108. *PubMed*. Web. 9 July 2015.

7. LaHaye, Stephanie, Joy Lincoln, and Vidu Garg. "Genetics of Valvular Heart Disease." *Current Cardiol Rep* 16 (2014): 1-9. *PubMed*. Web. 9 July 2015.

8. d'Arcy, J L., B D. Prendergast, J B. Chambers, S G. Ray, and B Bridgewater. "Valvular Heart Disease: The Next Cardiac Epidemic." *Heart* 97.2 (2011): 91-93. *PubMed*. Web. 16 Mar. 2015.

9. Eren, Esin, Hamit Y. Ellidag, Yesim Cekin, Raif U. Ayoglu, and Ali O. Sekercioglu. "Heart Valve Disease: The Role of Calcidiol Deficiency, Elevated Parathyroid Hormone Levels and Oxidative Stress in Mitral and Aortic Valve Insufficiency." *Redox Report* 19.1 (2014): 34-39. *PubMed*. Web. 9 July 2015.

10. Go AS, Mozaffarian D, Roger VL, Benjamin EJ, Berry JD, Borden WB, et al. Heart Disease and Stroke Statistics-2013 update: A Report from the American Heart Association. Circulation. 2013; 127:e6-e245.

11. Stewart BF, Siscovick D, Lind BK, et al. Clincial Factors Associated with Calcific Aortic Valve Disease. Cardiovascular Health Study. J Am Coll Cardiol 1997; 29 (3): 630-4.

12. *Statistical Abstract of the United States*. U. S. Census Bureau, 2012. Web. 16 Mar. 2015. <https://www.census.gov/compendia/statab/2012/tables/12s0009.pdf>.

13. Pibarot, Philippe, and Jean G. Dumesnil. "Valvular Heart Disease: Changing Concepts in Disease Management." *Circulation* 119 (2009): 1034-48. *PubMed*. Web. 16 Mar. 2015

14. Arjunon, Sivakkumar, Pablo H. Ardana, Neelakantam Saikrishnan, Shalv Madhani, and Brent Foster. "Design of a Pulsatile Flow Facility to Evaulate Thrombogenic Potential of Implantable Cardiac Devices." *Journal of Biomechanical Engineering* 137.4 (2015). *PubMed*. Web. 16 Mar. 2015.

15. Iyengar, Arun K., Hiroatsu Sugimoto, David B. Smith, and Michael S. Sacks. "Dynamic *In vitro* Quantification of Bioprosthetic Heart Valve Leaflet Motion Using Structured Light Projection." *Annals of Biomedical Engineering* 29 (2001): 963-73. *PubMed*. Web. 15 Mar. 2015.

16. Bloomfield, Peter. "Choice of Heart Valve Prosthesis." *Heart* 87 (2002): 583-89. *PubMed*. Web. 9 July 2015.

17. Walther T, Simon P, Dewey T, Wimmer-Greinecker G, Falk V, Kasimir MT, Doss M, Borger MA, Schuler G, Glogar D, Fehske W, Wolner E, Mohr FW, Mack M. Transapical minimally invasive aortic valve implantation: multicenter experience. *Circulation*. 2007;116(suppl):I-240–I-245.

18. Jaron, D, P Lelkes, and R Seliktar. *Mechanical Heart Valve*. The Body Synthetic, 17 Feb. 2008. Web. 13 July 2015. <http://www.pages.drexel.edu/~nag38/Types/ball.html>.

19. Matthews, Annette M. "The Development of the Starr-Edwards Heart Valve." *Texas Heart Institute Journal* 25 (1998): 282-93. *PubMed*. Web. 9 July 2015.

20. Lefrak EA, Starr A. Starr-Edwards Ball Valve In Cardiac Valve Prostheses. New York: Appleton-Century-Crofts, 1979:67-117.

21. Swanson JS, Starr A. The Ball Valve Experience Over Three Decades. Ann Thorac Surg 1989; 48: S51-52.

22. Tarzia, Vincenzo, Tomaso Bottio, Luca Testolin, and Gino Gerosa. "Extended (31 Years) Durability of a Starr-Edwards Prosthesis in Mitral Position." *European Association for Cardio-Thoracic Surgery* (2007): 570-71. *PubMed*. Web. 9 July 2015.

23. Vlahakes, Gus J. "Mechanical Heart Valves: The Test of Time." *Circulation* 116 (2007): 1759-60. *PubMed*. Web. 9 July 2015.

24. Akins, C W. "Medtronic-Hall Prosthetic Aortic Valve." *Semin Thorac Cardiovas Surg* 8.3 (1996): 242-48. *PubMed*. Web. 9 July 2015.

25. Wu, Ying X., Eric G. Butchart, Jeffrey S. Borer, Ajit Yoganathan, and Gary L. Gunkemeier. "Clinical Evaluation of New Heart Valve Prostheses: Update of Objective Performance Criteria." *Ann Thorac Surg* 98 (2014): 1865-74. *PubMed*. Web. 13 July 2015.

26. Streckenbach, Scott. "Prosthetic Valves." : 1-56. *PubMed*. Web. 9 July 2015.

27. Svennevig, Jan L., Michel Abdelnoor, and Sigurd Nitter-Hauge. "Twenty-Five-Year Experience With the Medtronic-Hall Valve Prosthesis in the Aortic Position: A Follow-Up Cohort Study of 816 Consecutive Patients." *Circulation* 116 (2007): 1795-800. *PubMed*. Web. 9 July 2015.

28. Ozer, Kandemir, Tokmakoglu Hilmi, Yildiz Ulku, Tezcaner Tevfik, and Yorgancioglu C. A. "St. Jude Medical and CarboMedics Mechanical Heart Valves in the Aortic Position." *Texas Heart Institute Journal* 33 (2006): 154-59. *PubMed*. Web. 9 July 2015.

29. Emery, Robert W., Christopher C. Krogh, Kit V. Arom, Ann M. Emery, and Kathy Benyo-Albrecht. "The St. Jude Medical Cardiac Valve Prosthesis: A 25-Year Experience with Single Valve Replacement." *The Society of Throacic Surgeons* (2005): 776-83. *PubMed*. Web. 9 July 2015.

30. Myken, Pia S., and Odd Bech-Hansen. "A 20-Year Experience of 1712 Patients With the Biocor Porcine Bioprosthesis." *The Journal of Thoracic and Cardiovascular Surgery* (2009): 76-81. *PubMed*. Web. 8 July 2015.

31. McClure, R S., Narendren Narayanasamy, Esther Wiegerinck, Stuart Lipsitz, and Ann Maloney. "Late Outcomes for Aortic Valve Replacement With the Carpentier-Edwards Pericardial Bioprosthesis: Up to 17-Year Follow-Up in 1,000 Patients." *Ann Thorac Surg* 89 (89): 1410-16. *PubMed*. Web. 9 July 2015.

32. *Types of Replacement Heart Valves*. American Heart Association, 30 Jan. 2015. Web. 16 Mar. 2015. <https://www.heart.org/HEARTORG/Conditions/More/HeartValveProblemsandDisease/Types-of-Replacement-Heart-Valves_UCM_451175_Article.jsp>.

33. Dasi, Lakshmi P., Helene A. Simon, Philippe Sucosky, and Ajit P. Yoganathan. "Fluid Mechanics of Artificial Heart Valves." *Clinical Experimental Pharmacology Physiology* 36.2 (2009): 225-37. *PubMed*. Web. 16 Mar. 2015.

34. Bonow RO, Carabello BA, Kanu C, de Leon AC Jr, Faxon DP, Freed MD, Gaasch WH, Lytle BW, Nishimura RA, O'Gara PT, O'Rourke RA, Otto CM, Shah PM, Shanewise JS, Smith SC Jr, Jacobs AK, Adams CD, Anderson JL, Antman EM, Faxon DP, Fuster V, Halperin JL, Hiratzka LF, Hunt SA, Lytle BW, Nishimura R, Page RL, Riegel B. ACC/AHA 2006 guidelines for the management of patients with valvular heart disease: a report of the American College of Cardiology/American Heart Association Task Force on Practice Guidelines. *Circulation*. 2006;114:e84–e231.

35. Vesey JM, Otto CM. Complications of prosthetic heart valves. *Curr Cardiol Rep*. 2004;6:106 –111.

36. Jun, Brian H., Neelakantan Saikrishnan, Sivakkumar Arjunon, B M. Yun, and Ajit P. Yoganathan. "Effect of Hinge Gap Width of a St. Jude Medical Bileaflet Mechanica Heart Valve on Blood Damage Potential - An In Vitro Micro Particle Image Velocimetry Study." *Journal of Biomechanical Engineering* 136 (2014): 1-11. *PubMed*. Web. 13 July 2015.

37. Jun, Brian H., Neelakantan Saikrishnan, and Ajit P. Yoganathan. "Micro Particle Image Velocimetry Measurements of Steady Diastolic Leakage Flow in the Hinge of a St. Jude Medical Refent Mechanical Heart Valve." *Annals of Biomedical Engineering* 42.3 (2014): 526-40. *PubMed*. Web. 13 July 2015.

38. Simon, Helene A., Liang Ge, Fotis Sotiropoulos, and Ajit P. Yoganathan. "Numerical Investigation of the Performance of Three Hinge Designs of Bileaflet Mechanical Heart Valves." *Annals of Biomedical Engineering* 38.11 (2010): 3295-310. *PubMed*. Web. 13 July 2015.

39. Kuan, Yee H., Foad Kabinejadian, Vinh-Tan Nguyen, Boyang Su, and Ajit P. Yoganathan. "Comparison of Hinge Microflow Fields of Bileaflet Mechanical Heart Valves Implanted in Different Sinus Shape and Downstream Geometry." *Computer Methods in Biomechanics and Biomedical Engineering* 18.16 (2015): 1785-96. *PubMed*. Web. 13 July 2015.

40. Ellis Jt, Healy TM, Fontaine AA, Saxena R, Yoganathan AP. Velocity Measurements and Flow Patterns Within the Hinge Region of a Medtronic Parallel Bileaflet Mechanical Valve With Clear Housing. *J Heart Valve Dis.* 1996; 5: 591-9.

41. Grunkemeier JM, Tsai WB, McFarland CD, and Horbett T a. 2000. The effect of adsorbed fibrinogen, fibronectin, von Willebrand factor and vitronectin on the procoagulant state of adherent platelets. *Biomaterials* 21(22):2243–52.

42. Holme PA, Orvin U, Hamers MJ, Solum NO, Brosstad FR, Barstad RM, and Sakariassen KS. 1997. Shear-Induced Platelet Activation and Platelet Microparticle Formation at Blood Flow Conditions as in Arteries With a Severe Stenosis. *Arteriosclerosis, Thrombosis, and Vascular Biology* 17:646–653.

43. George JN. 2000. Platelets. *The Lancet* 355(9214):1531–1539.

44. Hammermeister K, Sethi GK, Henderson WG, Grover FL, Oprian C, Rahimtoola SH. Outcomes 15 years after valve replacement with a mechanical versus a bioprosthetic valve: final report of the Veterans Affairs randomized trial. *J Am Coll Cardiol*. 2000;36:1152–1158.

45. Weska, Raquel F., Cassiano G. Aimoli, Grinia M. Nogueira, Adolfo A. Leirner, and Marina J. Maizato. "Natural and Prosthetic Heart Valve Calcification: Morphology and Chemical Composition Characterization." *Artificial Organs* 34.4 (2010): 311-18. *PubMed*. Web. 9 July 2015.

46. Singhal, Pooja, Adriana Luk, and Jagdish Butany. "Bioprosthetic Heart Valves: Impact of Implantation on Biomaterials." *ISRN Biomaterials* (2013): 1-14. *PubMed*. Web. 9 July 2015.

47. Ishihara, Tokuhiro, Victor J. Ferrans, Michael Jones, Henry S. Cabin, and William C. Roberts. "Calcific Deposits Developing in a Bovine Pericardial Bioprosthetic Valve 3 Days After Implantation." *Circulation* 63.3 (1981): 718-23. *PubMed*. Web. 9 July 2015.

48. Bre, L P., R McCarthy, and W Wang. "Prevention of Bioprosthetic Heart Valve Calcification: Strategies and Outcomes." *Current Medicinal Chemistry* 27 (2014): 2553-64. *PubMed*. Web. 9 July 2015.

49. Schoen, Frederick J., and Robert J. Levy. "Calcification of Tissue Heart Valve Substitutes: Progress Toward Understanding and Prevention." *The Society of Throacic Surgeons* (2005): 1072-80. *PubMed*. Web. 9 July 2015.

50. Takano, Tamaki, Takamitsu Terasaki, Yuko Wada, Noburou Ohashi, and Kazunori Komatsu. "Early Bioprosthetic Valve Calcification with Alfacalcidol Supplementation." *Journal of Cardiothoracic Surgery* (2013): 8-11. *PubMed*. Web. 9 July 2015.

51. Barbarash, Olga, Natalya Rutkovskaya, Oksana Hryachkova, Evgenya Uchasova, and Anastasia Ponasenko. "Impact of Recipient-Related Factors on Structural Dysfunction of Xenoaortic Bioprosthetic Heart Valves." *Patient Preference and Adherence* 9 (2015): 389-99. *PubMed*. Web. 13 July 2015.

52. Mahjoub, Haifa, Patrick Mathieu, Eric Larose, Abdelaziz Dahou, and Mario Senechal. "Determinants of Aortic Bioprosthetic Valve Calcification Assessed by Multidetector CT." *Valvular Heart Disease* (2015): 472-77. *PubMed*. Web. 13 July 2015.

53. J. Butany and R. Leask, "The Failure Modes of Biological Prosthetic Heart Valves," *Journal of Long-Term Effects of Medical Implants*, vol. 11, no. 3-4, pp. 115-135, 2001.

54. Kim, Min-Seok, Saeromi Jeong, Hong-Gook Lim, and Yong J. Kim. "Differences in Xenoreactive Immune Response and Patterns of Calcification of Porcine and Bovine Tissues in a-Gal Knock-Out and Wild-Type Mouse Implantation Models." *European Journal of Cardio-Thoracic Surgery* (2014): 1-8. *PubMed*. Web. 13 July 2015.

55. Iyer, Anand, Paras Malik, Ramesh Prabha, Gana Kugathasan, and Opeyemi Kuteyi. "Early Postoperative Bioprosthetic Valve Calcification." *Heart, Lung and Circulation* 22 (2013): 873-74. *PubMed*. Web. 13 July 2015.

56. Meuris, B, H De Praetere, W Coudyzer, and W Flameng. "Evolving Bioprosthetic Tissue Calcification Can Be Quantified Using Serial Multislice CT Scanning." *International Journal of Biomaterials* (2013): 1-7. *PubMed*. Web. 13 July 2015.

57. Zhai, Wanyin, Xiqin Lu, Jiang Chang, Yanlin Zhou, and Hongfeng Zhang. "Quercetin-Crosslinked Porcine Heart Valve Matrix: Mechanical Properties, Stability, Anticalcification, and Cytocompatibility." *Acta Biomaterialia* 6 (2010): 389-95. *PubMed*. Web. 13 July 2015.

58. Sadowski, Jerzy, Krzysztof Bartus, Boguslaw Kapelak, Amy Chung, and Maciej Stapor. "Aortic Valve Replacement with Novel Anti-Calcification Technology Platform." *Kardiologia Polzka* 73.5 (2015): 317-22. *PubMed*. Web. 13 July 2015.

59. Levy, Robert J., Frederick J. Schoen, Willam B. Flowers, and S T. Staelin. "Initiation of Mineralization in Bioprosthetic Heart Valves: Studies of Alkaline Phosphate Activity and its Inhibition by AlCl3 or FeCl3 Preincubations." *Journal of Biomedical Materials Research* 25 (1991): 905-35. *PubMed*. Web. 9 July 2015.

60. "Replacement Heart Valve Guidance." *U.S. Food and Drug Administration*. FDA, 1994. Web. 9 Feb. 2015. <http://www.fda.gov/RegulatoryInformation/Guidances/ucm193096.htm>.

61. Lu, Po-Chien, Jia-shing Liu, Baoshu Xi, Jia Wu, and Ned H. Hwang. *On Accelerated Fatigue Testing of Prosthetic Heart Valves*. N.p.: Springer US, 2003. 185-96. Topics in Biomedical Engineering International Book Series. Springer Link. Web. 7 July 2015. <http://link.springer.com/chapter/10.1007%2F978-1-4419-8967-3_13>.

62. Riggan, Courtney N. "Charicterization of the Mitral Valve Using Accelerated Wear Testing." (2010): 1-80. *PubMed*. Web. 9 July 2015.

63. *Heart Valve Durability Tester*. Biomedical Device Consultants & Laboratories LLC, 2014. Web. 14 July 2015. <http://www.bdclabs.com/testing-equipment/heart-valve-durability-tester/>.

64. *HiCycle Durability Tester*. Vivitro Labs Inc., 2015. Web. 14 July 2015.
    <http://vivitrolabs.com/product/hicycle-durability-tester/>.

65. Yoganathan, Ajit P., Zhaoming He, and S C. Jones. "Fluid Mechanics of Heart Valves."
    Annu. Rev. Biomed. Eng. 6 (2004): 331-62. *PubMed*. Web. 14 July 2015.

66. Review article: Tissue engineering of semilunar heart valves: Current status and future
    development. J Heart Valve Dis 2004;13:272–80.

67. Dasi LP, Ge L, Simon HA, Sotiropoulos F, Yoganathan AP. Vorticity dynamics of a bileaflet
    mechanical heart valve in an axisymmetric aorta. Physics Fluids 2007:19.

68. Raffel, M., C.E. Willert, S.T. Wereley, J. Kompenhans. Particle image velocimetry: a
    practical guide. *Springer*. 1998.

69. Prasad, Ajay K. "Particle Image Velocimetry." *Current Science* 79.1 (2000): 51-60.
    PubMed. Web. 9 July 2015.

70. Grbic, S. et al. "Image-Based Computational Models for TAVI Planning." *Medical Image
    Computing and Computer-Assisted Intervention* 16.2 (2013): 395-402. Web. 10 Feb.
    2015.
    <https://books.google.com/books?id=gGC5BQAAQBAJ&pg=PA398&lpg=PA398&dq=aort
    ic+tissue+%22mass+density%22&source=bl&ots=qvg_MZImQ0&sig=ntgrlnTdrFDRrk4cFP
    79qNmKqm4&hl=en&sa=X&ei=VZEIVby5H4qoNtSdgyA&ved=0CC>.

71. Li, J, X Y. Luo, and Z B. Kuang. "A Nonlinear Anisotropic Model for Porcine Aortic Heart
    Valves." *Journal of Biomechanics* 34 (2001): 1279-89. *PubMed*. Web. 10 Feb. 2015.

72. Krucinski, S, I Vesely, M A. Dokainish, and G Campbell. "Numerical Simulation of Leaflet
    Flexure in Bioprosthetic Valves Mounted on Rigid and Expansile Stents." *Journal of
    Biomechanics* 26.8 (1992): 929-43. *PubMed*. Web. 10 Feb. 2015.

73. *Overview of Materials for Acrylic, Extruded*. MatWeb: Material Property Data, 2015.
    Springer Link. Web. 29 June 2015.
    <http://www.matweb.com/search/DataSheet.aspx?MatGUID=632572aeef2a4224b5ac8
    fbd4f1b6f77&ckck=1>.

74. Martin, Caitlin, and Wei Sun. "Simulation of Long-Term Fatigue Damage in Bioprosthetic
    Heart Valves: Effects of Leaflet and Stent Elastic Properties." *Biomech Model
    Mechanobiology* 13 (2014): 759-70. *PubMed*. Web. 11 July 2015.

75. Li, Kewei, and Wei Sun. "Simulated Thin Pericardial Bioprosthetic Valve Leaflet Deformation Under Static Pressure-Only Loading Conditions: Implications for Percutaneous Valves." *Annals of Biomedical Engineering* 38.8 (2010): 2690-701. *PubMed*. Web. 18 July 2015.

76. Sabbah, Hani N., Mohamed S. Hamid, and Paul D. Stein. "Estimation of Mechanical Stresses on Closed Cusps of Porcine Bioprosthetic Valves: Effects of Stiffening, Focal Calcium and Focal Thinning." *American Journal of Cardiology* 55 (1985): 1091-96. *PubMed*. Web. 18 July 2015.

77. Sabbah, Hani N., Mohamed S. Hamid, and Paul D. Stein. "Mechanical Stresses on Closed Cusps of Porcine Bioprosthetic Valves: Correlation with Sites of Calcification." *The Annals of Thoracic Surgery* 42.1 (1986): 93-96. *PubMed*. Web. 18 July 2015.

Education
Major(s) and Minor(s):   B.S. in Bioengineering
                            M.S. in Bioengineering

            Thesis Title: A STUDY IN THE DESIGN OF AN ACCELERATED WEAR TESTER THAT IS
                            COMPATIBLE WITH A PARTICLE IMAGE VELOCIMETRY AND HIGH SPEED
                            CAMERA SETUP

Thesis Supervisor: Keefe Manning

Work Experience

Date: August 2012 – Present
Title: Research Assistant
            Description:

                            Conducted experiments to determine a relationship between
                            fluid dynamics, cardiac assist devices, and platelet activation
                            Centrifuged and reconstituted bovine blood
                            Created blood bags containing heparin anticoagulant
                            Imaged platelets using confocal microscopy

Company: PSU Fluid Dynamics & Artificial Heart Lab
                                205 Hallowell Building, University Park, PA 16801
Supervisor's Name: Keefe Manning

Date: January 2012 – June 2012
Title: Clinical Engineering Intern
Description:

                            Conducted experiments assisting the clinical engineers'
                            research
                            Reorganized and maintained equipment logistics
                            Updated and maintained multiple informational databases
                            Created a training manual for future interns introducing them
                            to the Hearware Ventricular Assist Device

Company: Heartware Inc.
                                14400 NW 64th Avenue, Miami Lakes, FL 33014
Supervisor's Name: Neil Voskoboynikov

Awards

Penn State Summer Discovery Grant:
Supports undergraduate student engagement in original research, scholarship, and creative work

Penn State President's Freshman Award:
Presented to undergraduate degree candidates who have earned a 4.00 cumulative grade-point average based on a minimum of 12 Penn State credits completed by the end of fall semester

Publications

In-Vivo HVAD® Pump Flow Accuracy vs. Reference Flow Probe	Brown et al
International Society for Rotary Blood Pumps (ISRBP) Poster # 16	Istanbul, Turkey September 2012